HAL
open science

Testing Minimal Universal Extra Dimensions Using Higgs Boson Searches at the LHC

G. Belanger, A. Belyaev, M. Brown, M. Kakizaki, A. Pukhov

To cite this version:

G. Belanger, A. Belyaev, M. Brown, M. Kakizaki, A. Pukhov. Testing Minimal Universal Extra Dimensions Using Higgs Boson Searches at the LHC. Physical Review D, 2013, 87, pp.016008. hal-01126639

HAL Id: hal-01126639

https://hal.science/hal-01126639v1

Submitted on 6 Mar 2015

HAL is a multi-disciplinary open access archive for the deposit and dissemination of scientific research documents, whether they are published or not. The documents may come from teaching and research institutions in France or abroad, or from public or private research centers.

L'archive ouverte pluridisciplinaire **HAL**, est destinée au dépôt et à la diffusion de documents scientifiques de niveau recherche, publiés ou non, émanant des établissements d'enseignement et de recherche français ou étrangers, des laboratoires publics ou privés.

UT-HET-071

Testing Minimal Universal Extra Dimensions Using Higgs Boson Searches at the LHC

Geneviève Bélanger,[1] Alexander Belyaev,[2,3] Matthew Brown,[2] Mitsuru Kakizaki,[4] and Alexander Pukhov[5]

[1]*LAPTH, Université de Savoie, CNRS, B.P.110, F-74941 Annecy-le-Vieux Cedex, France*

[2]*School of Physics & Astronomy, University of Southampton, UK*

[3]*Particle Physics Department, Rutherford Appleton Laboratory, Chilton, Didcot, Oxon OX11 0QX, UK*

[4]*Department of Physics, University of Toyama, 3190 Gofuku, Toyama 930-8555, Japan*

[5]*Skobeltsyn Institute of Nuclear Physics, Moscow State University, Moscow 119992, Russia*

arXiv:1207.0798v3 [hep-ph] 13 Dec 2012

Abstract

Large Hadron Collider (LHC) searches for the SM Higgs boson provide a powerful limit on models involving Universal Extra Dimensions (UED) where the Higgs production is enhanced. We have evaluated all one-loop diagrams for Higgs production $gg \to h$ and decay $h \to \gamma\gamma$ within "minimal" UED (mUED), independently confirming previous results, and we have evaluated enhancement factors for Higgs boson production and decay over the mUED parameter space. Using these we have derived limits on the parameter space, combining data from both ATLAS and CMS collaborations for the most recent 7 TeV and 8 TeV LHC data. We have performed a rigorous statistical combination of several Higgs boson search channels which is important because mUED signatures from the Higgs boson are not universally enhanced.

We have found that $R^{-1} < 500$ GeV is excluded at 95% CL, while for larger R^{-1} only a very narrow ($\pm 1-4$ GeV) mass window around $m_h = 125$ GeV and another window (up to 2 GeV wide for $R^{-1} > 1000$ GeV) around $m_h = 118$ GeV are left. The latter is likely to be excluded as more data becomes available whereas the region around $m_h = 125$ GeV is where the recently discovered Higgs-like particle was observed and therefore where the exclusion limit is weaker.

It is worth stressing that mUED predicts an enhancement for all channels for $gg \to h$ production and decay while the vector boson fusion process $WW/ZZ \to h \to \gamma\gamma$ is generically suppressed and $WW/ZZ \to h \to WW^*/ZZ^*$ is standard. Therefore, as more 8 TeV LHC data becomes available, the information on individual Higgs boson production and decay processes provided by the CMS and ATLAS experiments can be effectively used to favour mUED or exclude it further.

I. INTRODUCTION

Theories with Universal Extra Dimensions (UED) are very promising for solving puzzles in the Standard Model (SM). The UED framework was proposed by Appelquist *et al* [1], following the suggestion of the existence of large (i.e. millimetre-scale) extra dimensions [2, 3] or a warped (Planck-scale) extra dimension [4]. In UED, unlike in the preceding extra dimension models, all SM particles are postulated to propagate in a TeV^{-1}-sized bulk (normal space plus the extra compactified dimensions). Models of UED provide solutions to problems such as explaining the three fermion generations in terms of anomaly cancellation [5], and providing a mechanism for a sufficient suppression of proton decay [6]. Moreover, UED models can naturally incorporate a $\mathbb{Z}_2$ symmetry called KK parity, analogous to R parity in supersymmetry, leading to a well-motivated dark matter candidate [7, 8].

The simplest UED theory is known as minimal Universal Extra Dimensions (mUED) and it posits a single, flat extra dimension compactified on an $S^1/\mathbb{Z}_2$ orbifold in order to recover chiral interactions in the 4D effective theory. Periodicity on a circle (S^1) leads to the discretisation of momentum along the extra dimension into integer multiples of the compactification scale, i.e. $p_5 = nR^{-1}$, where R is the radius of the circle. The integer n is called "Kaluza-Klein (KK) number" and is a conserved quantity[1] before orbifolding. The "orbifolding" to $S^1/\mathbb{Z}_2$ leads to KK number conservation being violated at loop level. However, KK *parity* – defined to be $(-1)^n$ – is conserved to *all* orders in perturbation theory. As a result of this symmetry, mUED predicts a stable lightest Kaluza-Klein particle (LKP) which would be a prospective candidate for dark matter.

The collider phenomenology of mUED has been studied intensively in many publications (e.g.[9–13]), but we are only aware[2] of one *experimental* paper [14] that has set LHC limits on mUED. This is not surprising – the search for mUED is much more difficult than the search of SUSY within the experimentally well-explored mSUGRA scenario at the LHC. The main reason for this is that mUED provides much smaller missing transverse momentum due to the small mass splitting between KK-partners of SM particles of the same KK level. Though dark matter constraints set an upper limit on the scale of mUED below about 1.6 TeV [15], this scale will be very difficult to test even with the 14 TeV LHC [13, 16]. More pragmatically, only a few computational tools for studying mUED are easily

[1] It is conserved in the following sense. Consider a vertex of three particles with KK numbers n, m and l. This vertex "conserves" KK number if $\pm n \pm m \pm l = 0$ can be satisfied for some (independent) choice of plus or minus signs. E.g. a $(1, 1, 0)$ vertex would conserve KK number, but $(0, 0, 1)$ would not.

[2] We thank Kohsaku Tobioka for bringing this work to our attention.

accessible to experimentalists: Datta *et al* [17] implemented mUED in `CompHEP`[18, 19]/`CalcHEP` [20, 21] and independent implementations [15, 16] have improved upon this by treating electroweak symmetry breaking consistently.

We show in this paper that the Higgs sector of mUED provides an excellent way of testing the model at the LHC as was shown recently in [22, 23]. Indeed the loop-induced production process $gg \to h$ and decay $h \to \gamma\gamma$ are sensitive to heavy KK particles and are thus different from their SM values. Here we improve on previous results by rigorously combining the limits from different channels ($gg \to h \to \gamma\gamma$, $gg \to h \to W^+W^- \to \bar{\ell}\nu\ell\bar{\nu}$ and $gg \to h \to ZZ \to 2\bar{\ell}2\ell$) statistically, using the latest ATLAS and CMS Higgs search results. Constraints on the mUED parameter space are then derived. Going beyond [22], we also show the effects of including the radiative mass corrections for these particles. Our independently-derived expressions for $gg \to h$ and $h \to \gamma\gamma$ amplitudes agree with those derived first by Petriello [24]

This paper is structured as follows. The next section describes the main features of the mUED model. In Sec. III, we evaluate and present the effect of KK-particles in the loop for $gg \to h$ production and Higgs decay to $\gamma\gamma$, W^+W^- and ZZ. The impact of KK-particles differ for each channel and this non-universality should be taken into account when establishing combined limits on the mUED parameter space. We express the results of that section in terms of the enhancement of the $gg \to h \to \gamma\gamma$, $gg \to h \to W^+W^-$ and $gg \to h \to ZZ$ cross-sections. Next, in Sec. IV B, we discuss how these results can be used to constrain the parameter space of the model, describing the problems encountered when statistically combining experimental data from different channels. In Sec. V we show new limits on the mUED parameter space using our rigorous statistical combination and the latest ATLAS and CMS data. Section VI contains our conclusions. Details on the calculation of the $gg \to h$ and $h \to \gamma\gamma$ amplitudes can be found in a set of appendices.

II. THE MUED MODEL

In UED, in contrast to other Kaluza-Klein theories, there is one or more towers of KK particles associated with *every* SM particle. The particles in a KK tower each have the same quantum numbers but progressively heavier masses. In mUED, to a good approximation, the mass of a KK particle is given in terms of its KK number by nR^{-1}, leading to a very regularly-spaced mass spectrum. At the tree level, this regular spacing is altered slightly by electroweak contributions m_0 to the mass so that

$$m_n^{\text{tree}} = \sqrt{n^2/R^2 + m_0^2}\,. \tag{1}$$

Furthermore, radiative corrections to the KK masses play a crucial role. Corrections to the masses of the strongly-interacting KK particles can be as large as 30% and, even for the weakly interacting particles for which the mass corrections are numerically small, radiative effects are extremely important. Without them there would be many nearly-degenerate particles and all the KK partners of (nearly) massless SM particles would be stable to a good approximation. Radiative corrections, first calculated in [25], lift the degeneracy. This means that all KK particles eventually decay to SM particles and the lightest KK particle (LKP), which is forbidden to decay to SM particles by KK parity conservation. This LKP (a heavy version of the photon for much of the parameter space) is an excellent dark matter candidate. The small mass splittings between KK-partners of SM particles of the same KK level leads to soft jets and leptons in the decay of KK-particles thus making it more challenging to extract a signal at the LHC.

Associated with the SM $W^{\pm}$ boson there is a single tower of KK partners $W_n^{\pm}$. However, each SM fermion f has *two* KK towers denoted $f_{1,2}^{(n)}$. This feature will be relevant when comparing the size of the contribution of bosons and fermions to the Higgs partial widths. Without electroweak and radiative corrections, these particles have simple interpretations: they are the KK partners of the $\mathrm{SU}(2)_L$ doublet and singlet respectively and only the left-handed (right-handed) components of f_1 (f_2) survive at the zero KK level after the orbifold projection.

The KK modes, on the other hand, are vector-like, i.e. their left- and right-handed components transform in the same way under SU(2). Another way to say this is that both components couple equally to the KK $W^{\pm}$ bosons. With electroweak and radiative effects included however, the mass eigenstates become mixtures of the electroweak eigenstates and so the couplings to the gauge bosons become chiral.

There are two free parameters in mUED: the Higgs mass m_h and the compactification scale R^{-1}. Strictly speaking, because mUED (like all theories involving extra dimensions) is not renormalisable it must be treated as an effective theory valid to some specified cut-off momentum scale Λ. Thus Λ is technically a third parameter of the theory. In practice, however, low energy observables are only weakly sensitive to the cut-off. For definiteness, in this paper, like in many of earlier works, as a benchmark point we take $\Lambda = 20R^{-1}$ which is low enough to keep the SM coupling constants perturbative below the cut-off scale [1, 26].[3]

[3] The vacuum stability condition constrains the cutoff scale $\Lambda R \lesssim 5$ for $R^{-1} \sim 1$ TeV and $m_h = 125$ GeV [27]. This bound can be evaded if the SM vacuum is metastable below the cutoff scale.

In mUED the Higgs mass is limited to be below around 230 GeV by the simple requirement that the dark matter candidate should be neutral [15, 28]. More stringent limits are derived from collider searches for the SM Higgs boson. Indeed as we will demonstrate in this paper, the signals from the Higgs boson in mUED are enhanced as compared to those of the SM in nearly all of the main search channels. One exception is the W-fusion production of the Higgs decaying to two photons. The LEP limit on the SM Higgs, $m_h > 114.4$ GeV, therefore provides a conservative lower limit. The LHC sensitivity to the Higgs within the mUED scenario is better than for the SM Higgs boson, leading to a reduced range of allowed masses as we will derive in the next sections. As we know, recently the discovery of the Higgs-like particle with m_h=125 GeV was claimed by both the CMS [29] and ATLAS [30] collaborations. This signal has a strong effect on the mUED parameter space and we use these latest CMS and ATLAS results (expressed in the form the limits on the SM Higgs parameter space) to limit mUED with m_h around 125 GeV. By the end of 2012 the LHC will be able to collect more statistics and clarify the nature of the Higgs-like particle which eventually could be applied to further uncover the status of mUED.

A lower bound of around 600 GeV on the compactification scale comes from tests of electroweak precision measurements [31] and $b \to s\gamma$ [32]. The upper bound on R^{-1} is provided by cosmological observations from the requirement that the abundance of the LKP (whose mass is approximately R^{-1}) does not exceed the observed dark matter abundance [15].

III. EVALUATION OF AMPLITUDES FOR HIGGS PRODUCTION AND DECAY IN MUED

In the SM, the dominant process for producing the Higgs boson at the LHC is gluon-gluon fusion, despite the leading order contribution being a one-loop process. This process, shown in Fig. 1 (left), involves triangle diagrams of quarks – predominantly the top quark because of its large Yukawa coupling. It is this large coupling and also the high gluon luminosity at the LHC that makes this production mechanism dominant. In mUED, KK quarks can also run in the triangle loop leading to an enhancement over the SM amplitude.

For low values of the Higgs mass (e.g. around the recently discovered [29, 30] Higgs-like particle at 125 GeV) the most powerful Higgs search channel is into two photons. Indeed the low QCD background for this process compensates for the fact that the Higgs decay width into two-photons is loop-induced and thus suppressed. In the SM the dominant contribution to the two-photon amplitude comes from

loops involving $W^\pm$ bosons. This contribution is about four times larger than the one from fermions. Furthermore, the charged fermion triangle loop (again, dominated by top quarks) interferes destructively with the $W^\pm$ contribution.

In mUED, new contributions arise from KK W's and KK fermions running in loops. The contributions of the KK W's and KK fermions have the same sign as their SM counterparts, but the increase as compared to the SM contribution is larger for fermions than for W's. First, associated with each SM fermion there are two towers of KK fermions while there is only one for $W^\pm$. Second, the contributions of particles from higher KK levels decrease more slowly for fermions than for W's, as we will see in the next section. Furthermore, for KK number $n \geq 1$, there is an additional contribution from charged scalars $a_n^\pm$. This field is a mixture of the KK modes of the 5th component of the charged vector field and the charged component of the Higgs field. At each KK level, the charged scalar contributes with the *same* sign as the fermion diagrams. The net effect is therefore to suppress the Higgs to diphoton decay rate relative to the SM prediction. The three (fermion, $W^\pm$ and $a_n^\pm$) contributions are shown in Fig. 1. Additional diagrams involving $W^\pm$ Goldstones and ghosts are presented in Appendix C.

In the following subsections we show the results of calculating the amplitude for production of a SM Higgs boson from gluon-gluon fusion, and also the amplitude for subsequent decay to two photons. The amplitudes $\mathcal{A}$ for the $gg \to h$ and $h \to \gamma\gamma$ processes both take the form

$$\mathcal{A} = \tilde{\mathcal{A}}\left[(p \cdot q)(\epsilon \cdot \eta) - (p \cdot \eta)(q \cdot \epsilon)\right], \tag{2}$$

where the external vector particles with momenta p and q have polarisation vectors ϵ and η respectively. These polarisation and momentum conventions are shown in Fig. 1.

In (2) the Higgs is allowed to be off-shell. To calculate the exact amplitude for $gg \to h \to \gamma\gamma$, one would combine the separate off-shell amplitudes for $gg \to h$ and $h \to \gamma\gamma$ with a Higgs propagator. However, in our analysis we use the "narrow width approximation" (valid when the Higgs boson's width is much less than its mass) which allows us to write the $gg \to h \to \gamma\gamma$ cross section as the product of the cross-section for production of an on-shell Higgs boson and the branching ratio of an on-shell Higgs to two photons, i.e.

$$\sigma(gg \to h \to \gamma\gamma) \approx \sigma(gg \to h) \times \mathrm{BR}(h \to \gamma\gamma).$$

In this approximation, we only need amplitudes involving on-shell Higgs bosons, so we can write (2) as

$$\mathcal{A} = \tilde{\mathcal{A}}\left[\frac{m_h^2}{2}(\epsilon \cdot \eta) - (p \cdot \eta)(q \cdot \epsilon)\right], \tag{3}$$

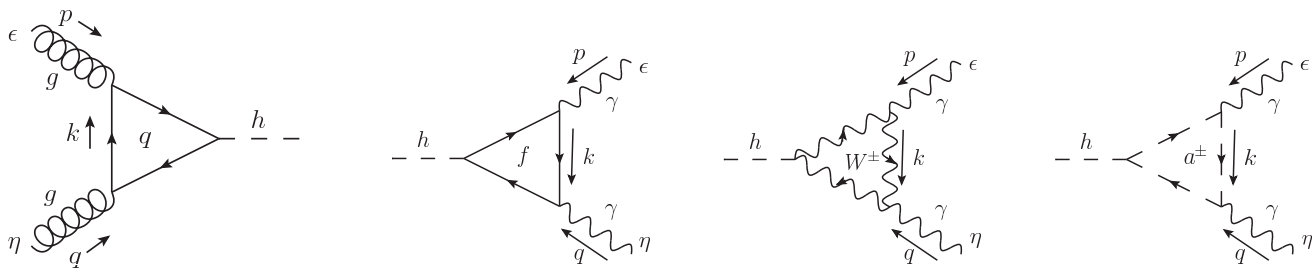

FIG. 1: Some diagrams involved in the production (left) and decay (right) of the SM Higgs boson. For the Higgs decay, there are also diagrams involving Goldstone bosons and Faddeev-Popov ghosts which are shown in appendix C.

where m_h is the Higgs mass.

These amplitudes have been calculated previously in the SM case in the $m_h/M \ll 1$ limit [33] (where M is the mass of the particle flowing in the loop) and subsequently [34] for general m_h/M. They have also been calculated in the mUED case (without radiative mass corrections) in [24]. We performed the calculation in the general mass case for mUED and included radiative corrections to the KK masses for the first time. We used the 't Hooft-Feynman gauge and regulated the divergences that appear in intermediate steps using dimensional regularisation. We made use of the well-known Passarino-Veltman functions [35] to evaluate the momentum integrals. Our calculation is shown in detail with all contributing diagrams in Appendices B and C. Our results reduce to the SM result found in the literature [36] when the KK modes are removed and agree with the result in [24] when we use tree-level KK masses in mUED.

A. Higgs production

The amplitude for $gg \to h$ (Fig. 1) reads[4]

[4] It should be noted that higher loop corrections to the $gg \to h$ amplitude can be substantial, reaching as much as 90% of the one-loop amplitude [37]. However, these large corrections are dominated by SM contributions (KK contributions are suppressed by powers of the compactification scale R^{-1}). The SM QCD corrections depend only on spin of the particle in the large mass limit and therefore they are universal for SM and mUED. In this paper we are ultimately only interested in the ratio of mUED and SM rates in which the QCD corrections cancel to a good approximation and therefore our results are valid for higher order QCD corrections.

$$\tilde{\mathcal{A}}_{ggh} = -\frac{\alpha_s}{4\pi v}\left(F_{ggh}^{\rm SM} + \sum_{n=1}^{N} F_{ggh}^{(n)}\right). \tag{4}$$

where α_s is the strong coupling constant and $v = 2\sin\theta_W m_W/e$ is the Higgs vacuum expectation value (θ_W is the Weinberg angle, e is the elementary electric charge and m_W is the mass of the W boson). In the SM there would be contributions from each quark flavour q in the loop, such that $F_{ggh}^{\rm SM} = \sum_q f_F(m_q)$ where the standard fermion contribution is given by

$$f_F(m) = \frac{8m^2}{m_h^2}\left[1 + \left(1 - \frac{4m^2}{m_h^2}\right)c_0(m)\right], \tag{5}$$

where c_0 is a dimensionless form of the scalar three-point Passarino-Veltman function

$$c_0(m) = \begin{cases} \left[\arcsin\left(\frac{m_h}{2m}\right)\right]^2 & m^2 \geq m_h^2/4 \\ -\frac{1}{4}\left[\ln\left(\frac{1+\sqrt{1-4m^2/m_h^2}}{1-\sqrt{1-4m^2/m_h^2}}\right) - i\pi\right]^2 & m^2 < m_h^2/4. \end{cases}$$

Note that f_F and c_0 are dimensionless functions and the argument m always appears in the dimensionless combination $4m^2/m_h^2$ (often written as τ in the literature).

In the $m \gg m_h$ limit, the above expressions reduce to $c_0 = \frac{m_h^2}{4m^2} + \frac{m_h^4}{48m^4} + \mathcal{O}(m_h^6/m^6)$ and

$$f_F(m) \approx \frac{4}{3} + \frac{m_h^2}{6m^2} + \mathcal{O}(m_h^4/m^4) \to 4/3. \tag{6}$$

Thus the amplitude tends to a constant in the heavy quark limit. This is however not the case when KK quarks are included in the loop: the heavy KK quarks "decouple" and, therefore, progressively higher KK modes lead to progressively smaller modifications to the Higgs boson coupling. Consequently, as we show below, one can safely neglect higher KK modes.

The reason for this decoupling is that, in contrast with SM fermions, while a KK particle's mass increases with KK number there is *no* corresponding increase in its Yukawa couplings and so decoupling does occur because of suppression from the propagators. This decoupling behaviour is shown explicitly below.

In mUED, the contribution from KK quarks at the nth KK level (there are two KK quarks at each level for each SM quark q) is

$$F_{ggh}^{(n)} = \sum_q \sin(2a_q^{(n)})\left(\frac{m_q}{m_{q,1}^{(n)}} f_F(m_{q,1}^{(n)}) + \frac{m_q}{m_{q,2}^{(n)}} f_F(m_{q,2}^{(n)})\right). \tag{7}$$

where $m_{q,1}^{(n)}$ and $m_{q,2}^{(n)}$ denote the KK quark masses and $a_q^{(n)}$ denote the mixing angles required to diagonalise the KK quark mass matrices. At tree level, all KK quark masses are nearly degenerate,

$$m_{q,\rm tree}^{(n)} = \sqrt{m_q^2 + \frac{n^2}{R^2}},$$

where m_q is the zero mode mass. Radiative corrections induce mass splittings between the KK fermions (see e.g. [25]). Similarly, the mixing angles are

$$a^{(n)}_{q,\text{tree}} = \frac{1}{2}\arctan\left(\frac{m_q R}{n}\right)$$

at tree-level (so $\sin(2a^{(n)}_{q,\text{tree}}) = m_q/m^{(n)}_{q,\text{tree}}$), but radiative corrections alter this expression (see for example [16]).

In our analysis we used one-loop corrected expressions for all masses and mixings as detailed in [25], but it is illustrative to neglect loop corrections and study the behaviour (just considering the top-quark contribution, which is dominant) for that case that $m_t^{(n)} > m_t > m_h$:

$$F^{(n)}_{ggh} \approx 2\left(\frac{m_t}{m_t^{(n)}}\right)^2 f_F(m_t^{(n)}) \approx 2\left(\frac{m_t}{m_t^{(n)}}\right)^2 \times \frac{4}{3}, \tag{8}$$

throwing away terms in m_h/m_t and $m_t R$ of order 3 or higher. This demonstrates the fact, mentioned above, that (in contrast to SM quarks) heavy KK quarks decouple from the process.

Taking the mass of the nth KK quark to be approximately n/R and considering just the top quark, the total KK contribution to the amplitude is approximately

$$F^{\text{KK}}_{ggh} \equiv \sum_{n=1}^{N} F^{(n)}_{ggh} \approx 2 \times \frac{4}{3} m_t^2 R^2 \sum_{n=1}^{N} \frac{1}{n^2}. \tag{9}$$

The sum is convergent as $N \to \infty$, thanks to the decoupling of the heavy KK particles. In this limit, $F^{\text{KK}}_{ggh} \to 4(\pi m_t R)^2/9$. So the momentum cutoff uncertainty is quite mild if one chooses a reasonably large value for it.

The sum over KK modes n is taken up to a cutoff N, corresponding to a momentum cutoff in the extra dimension of NR^{-1}. Mild cutoff-dependence is expected in perturbatively non-renormalisable theories such as mUED. In our quantitative analysis we chose $N = 20$ and included only t and b in the sum over quark flavours q, which is an excellent approximation due to the size of their Yukawa couplings compared to those of the lighter quarks. One should note that for large N the rest of the sum is proportional to $1/N$. Therefore, for $N = 20$ our result is given with about 5% accuracy as compared to the full sum.

B. Higgs decay to two photons

The $h \to \gamma\gamma$ amplitude is given by

$$\tilde{\mathcal{A}}_{h\gamma\gamma} = -\frac{\alpha}{2\pi v} F_{h\gamma\gamma}, \tag{10}$$

where α is the fine structure constant, v is the Higgs vacuum expectation value (defined just below Eq. 4), and

$$F_{h\gamma\gamma} = F_{h\gamma\gamma}^{\rm SM} + \sum_{n=1}^{N} F_{h\gamma\gamma}^{(n)} \tag{11}$$

The SM part consists of a contribution from the $W^\pm$ vector bosons and fermions:

$$F_{h\gamma\gamma}^{\rm SM} = f_V(m_W) + \sum_f n_c Q_f^2 f_F(m_f). \tag{12}$$

The sum is taken over all SM fermions f, each with charge $Q_f e$, setting n_c to 3 for quarks and 1 for leptons. The fermion loop function f_F is the same as for the $gg \to h$ case, given in (5), and the vector function f_V (representing the $W^\pm$ and related Goldstone and ghost contributions) is

$$f_V(m) = -2 - 12\frac{m^2}{m_h^2} - 24\frac{m^2}{m_h^2}\left(1 - \frac{2m^2}{m_h^2}\right) c_0(m). \tag{13}$$

In the large mass limit this tends to a constant

$$f_V \approx -7 - \frac{m_h^2}{2m^2} + \mathcal{O}(m_h^4/m^4) \to -7, \tag{14}$$

showing that particles whose masses are proportional to their Yukawa couplings do not decouple from the process, just as we saw in (6) for the production amplitude.

At the nth KK level the amplitude receives contributions from KK charged fermions (two KK partners for each SM fermion) and the KK $W_n^\pm$ vector boson. There is also a contribution from the charged scalar $a_n^\pm$ that is not present at the SM level, so

$$F_{h\gamma\gamma}^{(n)} = f_F^{(n)} + f_V^{(n)} + f_S^{(n)}. \tag{15}$$

The fermion contribution is the same as the quark contribution (7) was for the Higgs production amplitude, up to colour and charge factors:

$$f_F^{(n)} = \sum_f n_c Q_f^2 \sin(2a_f^{(n)}) \left(\frac{m_f}{m_{f,1}^{(n)}} f_F(m_{f,1}^{(n)}) + \frac{m_f}{m_{f,2}^{(n)}} f_F(m_{f,2}^{(n)}) \right). \tag{16}$$

and so has a similar asymptotic behaviour to the one shown in (8). The sum over KK modes is therefore convergent as well.

The vector contribution is given in terms of the SM expression as follows and also decouples as $m_{W,n} \to \infty$, in contrast to the SM case:

$$f_V^{(n)} = \frac{m_W^2}{m_{W,n}^2} f_V(m_{W,n}) \approx -\frac{7m_W^2}{m_{W,n}^2} + \mathcal{O}(m_W^4/m_{W,n}^4) \to 0. \tag{17}$$

The scalar contribution is given by

$$f_S^{(n)}(m_{a,n}, m_{W,n}) = \left[\frac{2m_W^2}{m_{W,n}^2}\left(1 - \frac{2m_{a,n}^2}{m_h^2}\right) - 2\right]\left[1 - \frac{4m_{a,n}^2}{m_h^2}c_0(m_{a,n})\right]. \tag{18}$$

At tree-level, $m_{a,n} = m_{W,n}$ so, keeping m_W and m_h constant, as we increase the KK scalar's mass,

$$f_S^{(n)} \approx \frac{m_W^2}{m_{a,n}^2}\left(\frac{1}{3} + \frac{m_h^2}{6m_W^2}\right) + \mathcal{O}(m_W^4/m_{a,n}^4) \to 0, \tag{19}$$

again demonstrating decoupling behaviour in the large KK mass limit.

In the SM case we can use the limits when the mass of the particle flowing in the loop is large compared to the Higgs mass to estimate the relative contributions from fermions and vectors, noting that they have opposite signs. Including the charge and colour factors for the fermion case and considering only the top quark, the ratio is $|f_V|/|n_c Q_t^2 f_F| \approx 7/\frac{16}{9} \approx 3.9$. Following the same procedure for contributions from level n KK particles (taking their masses to be approximately n/R) we find not only that the vector and fermion contributions each have the same sign as their SM counterparts but also that the ratio of vector to fermion contributions is smaller than in the SM: recognising that there are *two* KK top quarks, $|f_V^{(n)}|/|f_F^{(n)}| \approx 3.9(m_W^2/2m_t^2) \approx 0.42$, i.e. less than 1. This suggests that the net effect of KK particles will be from the top quark contribution which will thus interfere destructively with the SM contribution from W's, reducing the overall amplitude. In addition, there is the charged scalar contribution which has the same sign as the fermion contribution, reducing the amplitude further. This indication of amplitude suppression is confirmed by the full calculation.

The dependence of the two amplitudes (4) and (10) on the two free parameters of mUED – m_h and the inverse compactification radius R^{-1} – is shown in Fig. 2. This clearly indicates that for a light Higgs the ggh coupling is enhanced while $h\gamma\gamma$ is suppressed as argued above. The R^{-1} dependence enters through the KK masses and mixing angles. We have calculated the amplitudes using tree-level KK masses (dashed lines) and loop-corrected values (solid lines).

C. Calculating the mUED cross-section enhancement

In order to constrain mUED using SM Higgs boson searches at the LHC, we first need to calculate the enhancement of cross-sections of Higgs production and subsequent decay in different channels. Here we consider the three most important channels in the low Higgs mass range: $gg \to h \to \gamma\gamma$, $gg \to h \to W^+W^- \to \bar{\ell}\nu\ell\bar{\nu}$ and $gg \to h \to ZZ \to 2\bar{\ell}2\ell$. We can work in the narrow width approximation

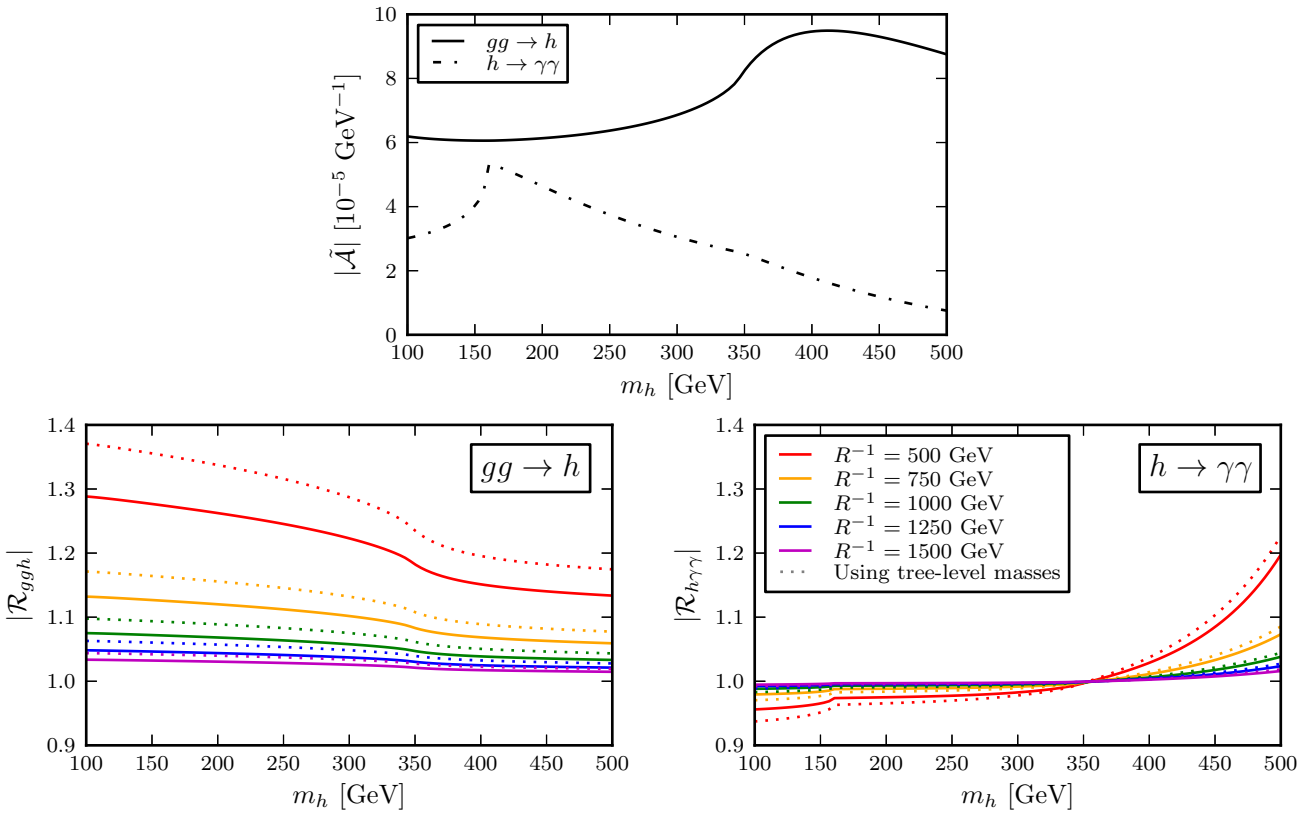

FIG. 2: Behaviour of the SM amplitudes and the relative sizes of the corresponding mUED amplitudes for several values of R^{-1}. The top figure shows the behaviour of the absolute values of the SM amplitudes for Higgs production and decay to two photons respectively. The bottom figures show the enhancement of these amplitudes in mUED relative to the SM, where $\mathcal{R} = \mathcal{A}_{\rm UED}/\mathcal{A}_{\rm SM}$. For the mUED plots, from top to bottom on the RHS of each plot: $R^{-1} = 500$, 750, 1000, 1250 and 1500 GeV. Solid lines show the results when using loop-corrected KK masses and dashed lines show tree-level results.

$\Gamma_h \ll m_h$, assuming that the Higgs is produced approximately on-shell and subsequently decays with some branching ratio BR, so that

$$\sigma(xx \to h \to yy) = \sigma(xx \to h) \times \mathrm{BR}(h \to yy).$$

In fact, since we need only the enhancement of each signal cross-section relative to the SM, knowledge of the full hadronic cross-section is not required because the integrals of parton density functions would be the same in mUED and the SM and would cancel in the ratio. The ratio can then be written simply (see, for example, [38]) in terms of total and partial Higgs widths as

$$\mu_{\gamma\gamma} \equiv \frac{\sigma_{\rm mUED}(gg \to h \to \gamma\gamma)}{\sigma_{\rm SM}(gg \to h \to \gamma\gamma)} \approx \frac{\Gamma_{\rm mUED}(h \to gg) \times \mathrm{BR}_{\rm mUED}(h \to \gamma\gamma)}{\Gamma_{\rm SM}(h \to gg) \times \mathrm{BR}_{\rm SM}(h \to \gamma\gamma)} \tag{20}$$

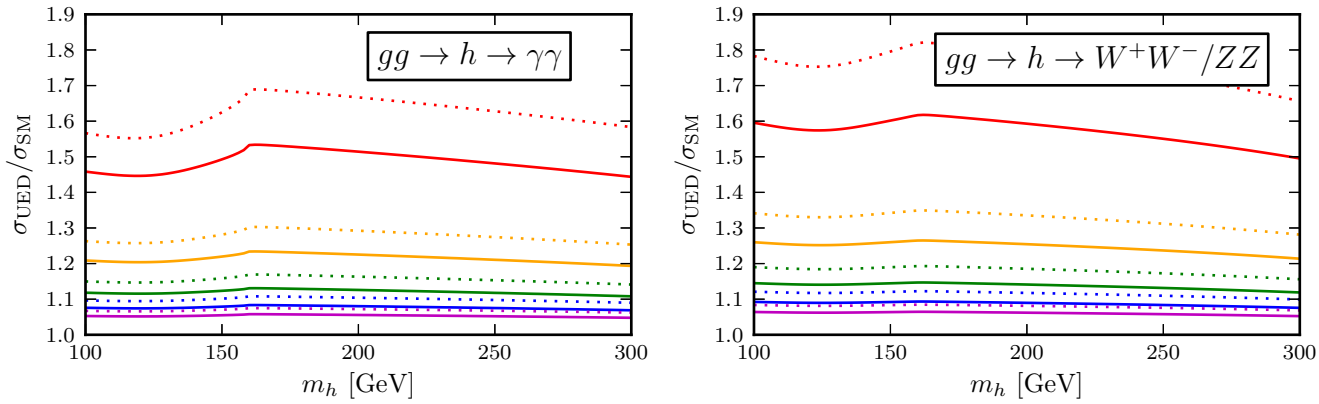

FIG. 3: Enhancement of mUED cross-sections in $\gamma\gamma$ (left) and W^+W^-/ZZ (right) channels relative to the SM. The graphs show variation with m_h for the following values of R^{-1}: from top to bottom on the RHS of each plot, $R^{-1} = 500$, 750, 1000, 1250 and 1500 GeV. Solid lines show results when using loop-corrected masses in the loops, while dashed lines correspond to tree-level masses.

for the diphoton channel and

$$\begin{aligned}\mu_{WW/ZZ} &\equiv \frac{\sigma_{\rm mUED}(gg \to h \to WW)}{\sigma_{\rm SM}(gg \to h \to WW)} \approx \frac{\Gamma_{\rm mUED}(h \to gg) \times {\rm BR}_{\rm mUED}(h \to WW)}{\Gamma_{\rm SM}(h \to gg) \times {\rm BR}_{\rm SM}(h \to WW)} \\ &\approx \frac{\Gamma_{\rm mUED}(h \to gg) \times \Gamma_{\rm SM}(h \to {\rm all})}{\Gamma_{\rm SM}(h \to gg) \times \Gamma_{\rm mUED}(h \to {\rm all})}\end{aligned} \tag{21}$$

for the W^+W^- and ZZ channels. Note that the mUED and SM expressions for the partial Higgs width to two vector bosons are the same, to leading order.

These two enhancement factors are plotted for various values of m_h and R^{-1} in Fig. 3, also showing the effect of including loop corrected masses in the loop diagrams.

IV. CONSTRAINING THE PARAMETER SPACE

A. Using one channel

Results for experimental searches for the Higgs boson at the LHC (by the ATLAS and CMS collaborations) are usually presented using "Brazil band" combined plots. These plots can be applied to family of models related to the SM in the following way. The pattern of fully-exclusive Higgs signal cross-sections ($\sigma(xx \to h \to yy)$) is the same as the Standard Model's except that each of them is scaled by some uniform factor, often denoted by μ. The plots show the value of this enhancement factor that

is excluded at the 95% confidence level for each value of the Higgs mass. This quantity is normally written as $\mu^{95\%}$. When $\mu^{95\%}$ drops below unity, the SM is excluded at the 95% confidence level.

Although $\mu^{95\%}$ can be used to exclude models that have the same pattern of cross-sections as the SM, for models (such as mUED) where different channels receive different corrections from new physics, this combined $\mu^{95\%}$ is not a useful quantity. Fortunately, the collaborations also provide exclusion plots for separate channels. It is then a simple matter to compare the value of, say, $\mu_{\gamma\gamma}$ to the excluded value $\mu_{\gamma\gamma}^{95\%}$. The exclusions from each channel and each experiment can then be overlapped in a simple way to constrain the model. As mentioned in the introduction, this has been done previously for mUED [22, 23]. However more accurate constraints on the model's parameter space can be obtained with a more sophisticated method of combining the exclusions from different channels in a statistically rigorous way. Such a method is discussed in the next section.

B. Statistical combination

We want to reproduce as closely as possible the analysis used by the experimental collaborations to calculate $\mu^{95\%}$ for the SM Higgs, but within the framework of mUED. We start completely analogously by imagining a family of models, each exactly the same as mUED except that the Higgs signal cross-sections in each channel are all scaled by a common factor μ. So, for example, if mUED (for certain values of m_h and R^{-1}) predicts a $gg \to h \to \gamma\gamma$ cross-section of $\sigma_{\gamma\gamma}^{\rm mUED}$, a $gg \to h \to WW \to \bar{\ell}\ell\bar{\nu}\nu$ cross-section of $\sigma_{WW}^{\rm mUED}$, and a $gg \to h \to ZZ \to \bar{2}\ell 2\ell$ cross-section of $\sigma_{ZZ}^{\rm mUED}$, we imagine a family of related models predicting $\{\mu\sigma_{\gamma\gamma}^{\rm mUED}, \mu\sigma_{WW}^{\rm mUED}, \mu\sigma_{ZZ}^{\rm mUED}\} = \{\mu\mu_{\gamma\gamma}\sigma_{\gamma\gamma}^{\rm SM}, \mu\mu_{WW}\sigma_{WW}^{\rm SM}, \mu\mu_{ZZ}\sigma_{ZZ}^{\rm SM}\}$, writing the cross-sections in terms of the mUED enhancement factors defined in (20) and (21).

We then construct functions giving the probability of observing a particular numbers of events in each channel (the "individual likelihoods", $p_i \equiv p(n_i^{\rm obs}|\mu, \mu_i)$). These will depend on the expected number of events in each channel i, given by

$$n_i = s_i + b_i = \mathcal{L}\varepsilon_i\mu\mu_i\sigma_i^{\rm SM} + b_i.$$

Here, s_i and b_i denote the total number of signal and background events in channel i expected to be observed in the model defined by (m_h, R^{-1}, μ). The integrated luminosity is given by $\mathcal{L}$ and the signal cross-section can be written as $\mu\mu_i\sigma_i^{\rm SM}$. Finally, it should be noted that the number of events one is able to see differs from the number of events that occur because of detector inefficiencies, particle misidentification and kinematical cuts. This is taken into account by the "efficiency" factor ε_i.

Once the individual likelihoods $p_i = p(n_i^{\rm obs}|\mu,\mu_i)$ are known, the total joint likelihood $P(\{n_i^{\rm obs}\}|\mu,\{\mu_i\}) = \prod_i p_i$ can be easily formed and then $\mu^{95\%}$ can be calculated.

The difficulty comes in reconstructing the likelihoods. The experimental collaborations do not routinely make available the efficiency factors, exact number of observed events after cuts, or expected number of background events after cuts. What they *do* make available is the value of $\mu_i^{95\%}$ for many of the channels, and also the "expected" $\mu_{i,\,\rm expected}^{95\%}$, which is the probability that the number of observed events might fluctuate down to the background-only expectation.

Azatov *et al* propose [39] a method for approximately reconstructing the individual channel likelihoods from the data provided by the experimental collaborations. We have followed their method in this paper, and explain some important points here.

It is possible to write the likelihood approximately as

$$p_i \propto \exp\left[-\frac{(n_i^{\rm obs}-n_i)^2}{2n_i^{\rm obs}}\right] \propto \exp\left[-\frac{(\mu\mu_i-\beta_i)^2}{2\alpha_i^2}\right],$$

when $n_i^{\rm obs} \gg 1$ (in fact $n_i^{\rm obs} > 10$ is a good approximation). Here we have introduced the following quantities:

$$\alpha_i \equiv \frac{\sqrt{n_i^{\rm obs}}}{s_i^{\rm SM}} \quad \text{and} \quad \beta_i \equiv \frac{n_i^{\rm obs}-b_i}{s_i^{\rm SM}}, \quad \text{where} \quad s_i^{\rm SM} = \mathcal{L}\varepsilon_i\sigma_i^{\rm SM}.$$

The important point to realise is that we have managed to write the three unknown quantities $n_i^{\rm obs}$, b_i and ε_i in just two independent combinations, α_i and β_i.

Making the further reasonable approximation that $(n_i^{obs}-b_i)/b_i \ll 1$ we can deduce, as shown in eq. 3.24 in [39], that

$$\alpha_i \approx \frac{\sqrt{b_i}}{s_i^{\rm SM}} = \frac{\mu_{i,\,\rm expected}^{95\%}}{1.96}$$

if we interpret exclusion limits in the Bayesian sense. With this knowledge we can then infer the value of β_i from the *observed* $\mu_i^{95\%}$, provided by the experimental collaborations, by solving the following equation (eq. 3.22 in [39]) numerically:

$$0.95 \approx \frac{\mathrm{Erf}\left(\frac{\mu_i^{95\%}-\beta_i}{\sqrt{2}\alpha_i}\right) + \mathrm{Erf}\left(\frac{\beta_i}{\sqrt{2}\alpha_i}\right)}{1+\mathrm{Erf}\left(\frac{\beta_i}{\sqrt{2}\alpha_i}\right)},$$

where the error function $\mathrm{Erf}(x) = \frac{2}{\sqrt{\pi}}\int_0^x \mathrm{e}^{-t^2}\mathrm{d}t$.

With the individual likelihoods approximately reconstructed in this way we can form the joint likelihood and calculate the combined $\mu^{95\%}$ (again, working in the Bayesian picture). We find it to be

$$\mu^{95\%} = \beta_{\rm comb} + \sqrt{2}\alpha_{\rm comb} \times \mathrm{Erf}^{-1}\left[0.95 - 0.05 \times \mathrm{Erf}\left(\frac{\beta_{\rm comb}}{\sqrt{2}\alpha_{\rm comb}}\right)\right],$$

where

$$\alpha_{\rm comb} \equiv \left(\sum_i \frac{\mu_i^2}{\alpha_i^2} \right)^{-\frac{1}{2}}$$

and

$$\beta_{\rm comb} = \alpha_{\rm comb}^2 \times \sum_i \frac{\mu_i \beta_i}{\alpha_i^2}.$$

Using the procedure outlined above, we performed a scan over the mUED parameter space, calculating $\mu^{95\%}$ for each point (m_h, R^{-1}). We used the $gg \to h \to \gamma\gamma$, $gg \to h \to W^+W^- \to \bar{\ell}\ell\bar{\nu}\nu$ and $gg \to h \to ZZ \to 2\bar{\ell}2\ell$ channels from ATLAS and CMS Higgs boson searches. We scanned m_h in 2-GeV steps, R^{-1} in 12.5-GeV steps. We have further considered additional constraints on the parameter space. The Higgs mass range is bound from below by LEP limits and from above by the requirement that the dark matter candidate be neutral – see [15]. The inverse radius must be greater than around 600 GeV so as not to conflict with electroweak precision tests [31, 32], and less than 1600 GeV so that the dark matter candidate is not too heavy [15].

V. RESULTS

Using our model's predictions of Higgs production enhancement for different values of m_h and R^{-1} together with experimental limits on Higgs boson production, we can exclude regions of the (m_h, R^{-1}) plane where $\mu^{95\%} < 1$. Initially, we statistically combined the CMS data from Fig. 6 (top) of [40] and the ATLAS data from Fig. 3 of [41] in each of the $\gamma\gamma$, W^+W^- and ZZ channels. Note that these data are from the old 7 TeV dataset, before the discovery of a Higgs-like particle at 125 GeV in July 2012. When we started writing this paper, this was the state of the art. We update the analysis using the newest 8 TeV data later in this section.

The resulting limits on mUED from the 7 TeV dataset are shown in our Fig. 4 (left), where the green contour separating the green and red shaded regions corresponds to $\mu^{95\%} = 1$ level. The other contours of constant $\mu^{95\%}$ are shown in steps of 0.05 for increasing value of $\mu^{95\%}$ towards the green region and its decreasing value in the opposite direction. The red-shaded region of the parameter space is excluded at 95% confidence level. These constraints are combined with other constraints from DM relic density [15] as well as EW precision tests [31] in Fig. 4 (right).

We can see that Higgs searches powerfully constrain mUED, in which Higgs production is enhanced. Compared to previous studies [22] we have included mass corrections for the particles in the loops, providing more realistic predictions of mUED cross sections, and have accurately combined non-universal

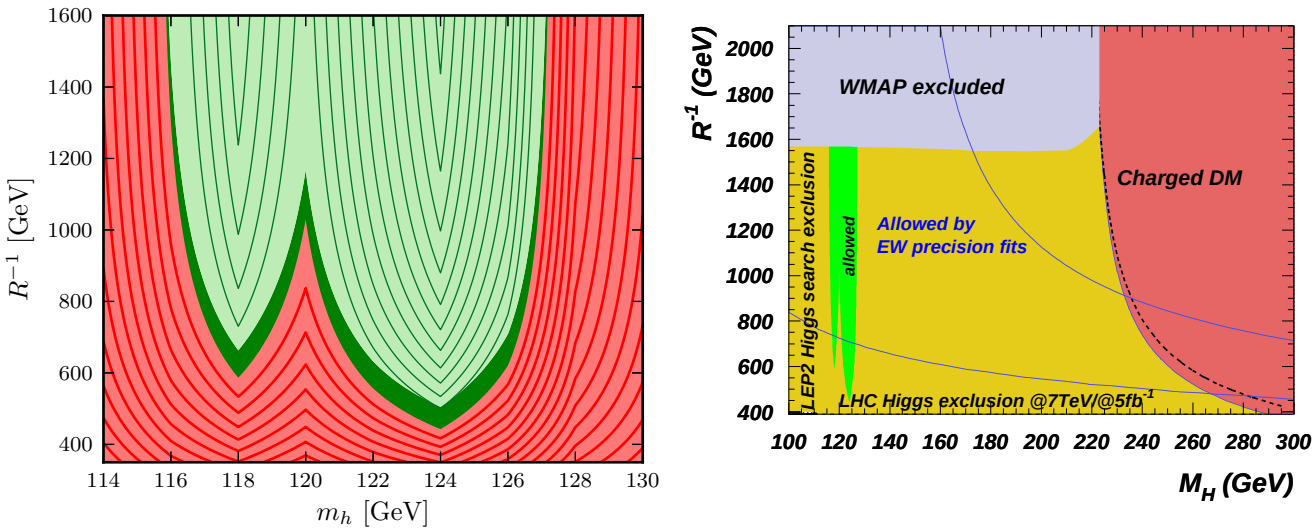

FIG. 4: Left: exclusion of mUED (m_h, R^{-1}) parameter space at 95% CL from Higgs boson search using combined ATLAS and CMS limits in $\gamma\gamma$, W^+W^- and ZZ channels, based on the 7 TeV data. The allowed region is in light green and the excluded region is in red. Dark green shows the additional allowed region when loop corrected KK masses are used instead of tree-level masses. Contours of constant $\mu^{95\%}$ are shown in steps of 0.05. Right: Combination of limits on the mUED parameter space from: the Higgs constraints considered in this paper; EW precision tests (95% CL); and DM relic density limits for $\Lambda = 40R^{-1}$ (solid line) and $\Lambda = 20R^{-1}$ (dashed line) cases.

enhancement for $\gamma\gamma$ and W^+W^-/ZZ signatures.

This new approach allows us to find accurate limits on the mUED (m_h, R^{-1}) parameter space. After combination of ATLAS and CMS limits for each individual channel ($\gamma\gamma$, W^+W^- and ZZ) in gluon-gluon fusion, we find that $R^{-1} < 500$ GeV is excluded at 95%CL. For 500 GeV $< R^{-1} <$ 600 GeV only a very narrow ($\pm 1 - 3$ GeV) mass window around $m_h = 125$ GeV is left. This is the region where the excess of the events in the Higgs search channels is reported by the ATLAS and CMS collaborations and where the exclusion limit is weaker. For even larger values of R^{-1} another narrow mass range around $m_h = 118$ GeV is allowed.

For a Higgs mass $m_h = 125$ GeV, we display in Fig. 5 the variation of the enhancement factor in the $gg \to h \to \gamma\gamma$ (top) and $gg \to h \to W^+W^-/ZZ$ (middle) channels as a function of R^{-1} together with the suppression factor in the $W^+W^-/ZZ \to h \to \gamma\gamma$ (bottom). The latter is relevant for the Higgs search in the $pp \to jj\gamma\gamma$. These plots can be used to ascertain how a measurement of each

channel's cross-section can be used to constrain the scale R^{-1}. For example, an enhancement in both the $gg \to h \to \gamma\gamma$ and the $gg \to h \to W^+W^-$ channel would favour the mUED model around the TeV scale while a large enhancement in $pp \to jj\gamma\gamma$ would disfavour the model.

Since we started to write this paper, new limits (calculated from the first tranche of 8 TeV data) have been released by CMS [29] and ATLAS [30]. The data are strong enough for each experiment to claim discovery of a Higgs-like particle with a mass of around 125 GeV, confirming the hints evident in earlier analyses. The new ATLAS limits are shown for all channels in Fig. 16a of the supplementary figures associated with [30].[5] CMS make their latest limits for $\gamma\gamma$ available in Fig. 4a of [42] and their limits for WW in Fig. 4 (right) of [29]. The CMS limits for the $h \to ZZ \to 4\ell$ channel can be found in the supplementary figures for [43].[6]

We have calculated the constraints on the mUED parameter space in light of these new experimental data and the result is shown in Fig. 6 (left). We also show a comparison of the allowed regions for the old and new data in Fig. 6 (right).

We should also comment on the expected sources of uncertainty in our approach. Since our study is based on the *ratio* of mUED and SM cross-sections our results are insensitive to PDF uncertainties which simply cancel in this ratio. The other potential sources of uncertainty are the higher order corrections to the amplitudes we calculate. Fortunately, higher order corrections has been evaluated for $h \to gg$ process to four loops in [44]. Using the results from that paper one can estimate that the biggest uncertainty in our results from higher order corrections comes from the second loop term, containing an additional $\log(m_q^{(n)}/m_h)$ dependence due to mUED. It turns out numerically that this effect is about $1\% \times (\sigma_{mUED}/\sigma_{SM}) < 1\%$ and is thus negligible. Therefore the biggest source of uncertainty is actually related to the choice of using loop-corrected versus tree-level masses one in our loop calculations. As we argue above, we choose the loop-corrected mass for our evaluations, but in order to be on the conservative side we consider the impact of choosing the tree-level mass instead. We use this difference to estimate the uncertainty in our limits. With tree-level masses, our limits presented in both Fig. 4 and Fig. 6 are shifted by about 50 GeV. In fact the limits actually improve when using the tree-level masses.

The allowed region shrinks overall with the extra data, but the high and low m_h limits on R^{-1} *relax* down to about 550 GeV. This is actually to be expected: in the 2011 data, the W^+W^- channel

[5] These can be found at `https://atlas.web.cern.ch/Atlas/GROUPS/PHYSICS/PAPERS/HIGG-2012-27/`
[6] `https://twiki.cern.ch/twiki/bin/view/CMSPublic/Hig12016TWiki`

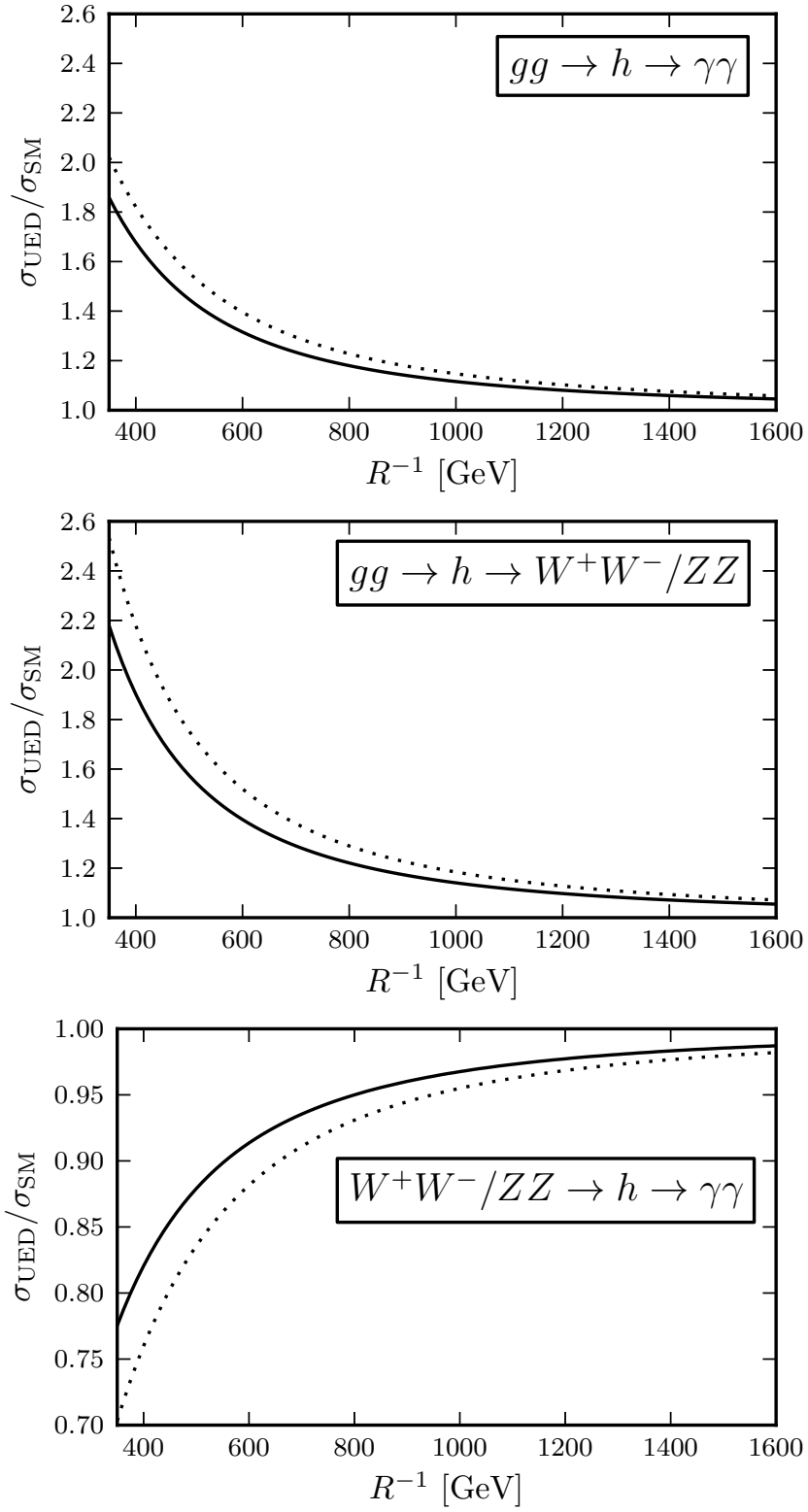

FIG. 5: The variation with respect to R^{-1} of the mUED cross-sections for $gg \to h \to \gamma\gamma$ (top), $gg \to h \to W^+W^-/ZZ$ (middle) and $W^+W^-/ZZ \to h \to \gamma\gamma$ (bottom) channels relative to the SM for $m_h = 125$ GeV. Solid lines show results when using loop-corrected masses in the loops, while dashed lines correspond to tree-level masses.

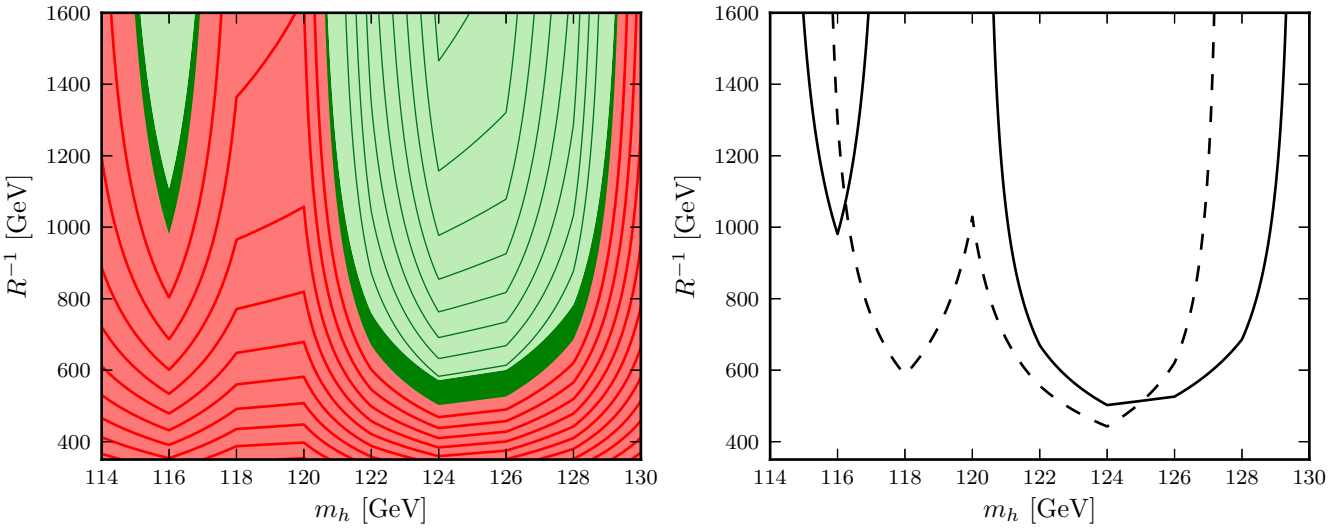

FIG. 6: Left: limits on mUED parameter space from newest 7 TeV and 8 TeV ATLAS and CMS Higgs search data using the same conventions as in Fig. 4 (left). Right: comparison of allowed regions for the combined 7 TeV and 8 TeV LHC data (solid) and 7 TeV data (dashed) using loop masses.

surprisingly showed no excess of events around 125 GeV even though such an excess was observed in the other channels, including ZZ. In the new data, there is an excess in W^+W^-, bringing this channel in line with the others and thus *weakening* the limit on the mUED parameter space slightly at the edges of the allowed region where the diphoton channel is less restrictive. However, the improvement in limiting power of the diphoton channel causes the region 117 GeV $\lesssim m_h \lesssim$ 121 GeV to become forbidden.

With the new data then, all values of $R^{-1} < 550$ GeV are forbidden, leaving a small region of allowed parameter space 2–8 GeV wide around $m_h = 125$ GeV and another allowed island up to 2 GeV wide around 116 GeV for $R^{-1} > 1000$ GeV.

VI. CONCLUSIONS

LHC searches for the SM Higgs provide a powerful limit on mUED model where the Higgs production is enhanced. We have evaluated all one-loop diagrams for Higgs production $gg \to h$ and decay $h \to \gamma\gamma$ within the mUED model and have independently confirmed previous results [24]. Based on these results we have derived enhancement factors for Higgs boson production and decay in the mUED parameter space. Then, using these factors we have derived the first limits on the mUED parameter space which combine both limits from ATLAS and CMS collaborations for 7 TeV and 8 TeV LHC data and take into

account statistical combination of several Higgs boson search channels properly. As for other extensions of the SM, the correct statistical combination of several Higgs boson search channels is important for mUED since these channels are not universally enhanced: the $gg \to h \to \gamma\gamma$ process is not enhanced as strongly as the $gg \to h \to WW^*$ or $gg \to h \to ZZ^*$ processes due to the fact that the decay $h \to \gamma\gamma$ is actually suppressed as compared to the Standard Model. Overall enhancement for $gg \to h \to \gamma\gamma$ nevertheless takes place because the enhancement of $gg \to h$ overcomes the suppression in the $h \to \gamma\gamma$ decay.

In contrast to previous studies [22] we have included mass corrections for the KK particles in the loop and found that the effect of KK particles is slightly reduced as compared to the calculation using tree-level masses. The comparison between the computations with tree-level and radiatively corrected masses provides information about the theoretical uncertainties in the enhancement of the Higgs boson production and decay within the mUED model. Also, we think that including these mass corrections gives more precise result and allows one to take into account some part of the higher order corrections. This is since one-loop corrected masses give a better approximation to pole masses and since the coupling constants that couple the gluon (or photon) to the KK quarks are protected by gauge invariance from receiving radiative corrections.

As a result we have found an accurate limit on mUED in the (m_h, R^{-1}) parameter space. After combination of ATLAS and CMS limits for each individual channel ($\gamma\gamma$, WW^* and ZZ^*) for the latest 7 TeV and 8 TeV data, we found that $R^{-1} < 550$ GeV is excluded at 95%CL, while for larger R^{-1} only a very narrow ($\pm 1 - 4$ GeV) mass window around $m_h = 125$ GeV (the mass of the recently observed Higgs-like particle), and another smaller window around 118 GeV (for $R^{-1} > 1000$ GeV) remain allowed.

As new 8 TeV data becomes available, the results from the different Higgs search channels can be used to fit the mUED parameter space. Signals compatible with the SM would eventually push the values of R^{-1} above the TeV scale while deviations from the SM could either be compatible with a lower scale or even exclude mUED completely depending on the channels involved. Indeed mUED predicts an enhancement for all channels for $gg \to h$ production and decay. On the other hand, the vector boson fusion process $WW/ZZ \to h \to \gamma\gamma$ is generically suppressed in mUED while $WW/ZZ \to h \to WW^*/ZZ^*$ is standard. A confirmation of the larger excess in the vector boson fusion mode over the gluon fusion mode for the two-photon channel that is currently observed would disfavour mUED. On the other hand predictions that come closer to the SM ones would lead to an increase in the mUED scale.

With detailed information on individual Higgs boson production and decay processes provided by

CMS and ATLAS experiments, one can understand much better the nature of the Higgs boson and interpret it within mUED or other BSM theories.

Acknowledgements

We would like to thank Aleksandr Azatov for useful discussion on the statistical methods. The work of GB, AP was supported in part by the GDRI-ACPP of CNRS. AB and MB thank the Royal Society for partial financial support. AB also thanks the NExT Institute and SEPnet for financial support. The work of AP was supported by the Russian foundation for Basic Research, grant RFBR-10-02-01443-a. The work of MK was supported in part by Toyama Prefecture Citizens' Personal Development Foundation (TPCPDF).

[1] T. Appelquist, H.-C. Cheng, and B. A. Dobrescu, Phys.Rev. **D64**, 035002 (2001), arXiv:hep-ph/0012100.

[2] N. Arkani-Hamed, S. Dimopoulos, and G. Dvali, Phys.Lett. **B429**, 263 (1998), arXiv:hep-ph/9803315.

[3] I. Antoniadis, N. Arkani-Hamed, S. Dimopoulos, and G. Dvali, Physics Letters B **436**, 257 (1998).

[4] L. Randall and R. Sundrum, Phys. Rev. Lett. **83**, 3370 (1999).

[5] B. A. Dobrescu and E. Poppitz, Phys. Rev. Lett. **87**, 031801 (2001), arXiv:hep-ph/0102010.

[6] T. Appelquist, B. A. Dobrescu, E. Ponton, and H.-U. Yee, Phys.Rev.Lett. **87**, 181802 (2001), arXiv:hep-ph/0107056.

[7] H.-C. Cheng, J. L. Feng, and K. T. Matchev, Phys.Rev.Lett. **89**, 211301 (2002), arXiv:hep-ph/0207125.

[8] G. Servant and T. M. Tait, Nucl.Phys. **B650**, 391 (2003), arXiv:hep-ph/0206071.

[9] C. Macesanu, C. McMullen, and S. Nandi, Phys.Rev. **D66**, 015009 (2002), arXiv:hep-ph/0201300.

[10] B. Bhattacherjee, A. Kundu, S. Rai, and S. Raychaudhuri, Physical Review D **81**, 035021 (2010), arXiv:0910.4082v1.

[11] D. Choudhury, A. Datta, and K. Ghosh, JHEP **08**, 051 (2010), arXiv:0911.4064.

[12] P. Bandyopadhyay, B. Bhattacherjee, and A. Datta, JHEP **03**, 048 (2010), arXiv:0909.3108.

[13] H. Murayama, M. Nojiri, and K. Tobioka, (2011), arXiv:1107.3369.

[14] The ATLAS Collaboration, CERN Report No. ATLAS-CONF-2011-155, 2011 (unpublished).

[15] G. Belanger, M. Kakizaki, and A. Pukhov, (2010), arXiv:1012.2577.

[16] A. Belyaev, M. Brown, J. Moreno, and C. Papineau, (in preparation).

[17] A. Datta, K. Kong, and K. T. Matchev, New J. Phys. **12**, 075017 (2010), arXiv:1002.4624.

[18] A. Pukhov *et al.*, hep-ph/9908288 (1999), arXiv:hep-ph/9908288.

[19] CompHEP Collaboration, E. Boos *et al.*, Nucl.Instrum.Meth. **A534**, 250 (2004), arXiv:hep-ph/0403113.

[20] A. Pukhov, (2004), arXiv:hep-ph/0412191.

[21] A. Belyaev, N. D. Christensen, and A. Pukhov, (2012), arXiv:1207.6082.

[22] K. Nishiwaki, K.-y. Oda, N. Okuda, and R. Watanabe, Phys.Lett. **B707**, 506 (2012), arXiv:1108.1764.

[23] G. Belanger, A. Belyaev, M. Brown, M. Kakizaki, and A. Pukhov, EPJ Web Conf. **28**, 12070 (2012), arXiv:1201.5582.

[24] F. J. Petriello, JHEP **05**, 003 (2002), arXiv:hep-ph/0204067.

[25] H.-C. Cheng, K. T. Matchev, and M. Schmaltz, Phys. Rev. **D66**, 036005 (2002), arXiv:hep-ph/0204342.

[26] G. Bhattacharyya, A. Datta, S. K. Majee, and A. Raychaudhuri, Nucl.Phys. **B760**, 117 (2007), arXiv:hep-ph/0608208.

[27] M. Blennow, H. Melbeus, T. Ohlsson, and H. Zhang, Phys.Lett. **B712**, 419 (2012), arXiv:1112.5339.

[28] S. Matsumoto and M. Senami, Phys.Lett. **B633**, 671 (2006), arXiv:hep-ph/0512003.

[29] CMS Collaboration, S. Chatrchyan *et al.*, Phys.Lett.B (2012), arXiv:1207.7235.

[30] ATLAS Collaboration, G. Aad *et al.*, (2012), arXiv:1207.7214.

[31] I. Gogoladze and C. Macesanu, Phys. Rev. **D74**, 093012 (2006), arXiv:hep-ph/0605207.

[32] U. Haisch and A. Weiler, Phys.Rev. **D76**, 034014 (2007), arXiv:hep-ph/0703064.

[33] J. R. Ellis, M. K. Gaillard, and D. V. Nanopoulos, Nucl.Phys. **B106**, 292 (1976).

[34] M. A. Shifman, A. Vainshtein, M. Voloshin, and V. I. Zakharov, Sov.J.Nucl.Phys. **30**, 711 (1979).

[35] G. 't Hooft and M. Veltman, Nucl.Phys. **B153**, 365 (1979).

[36] A. Djouadi, Phys.Rept. **457**, 1 (2008), arXiv:hep-ph/0503172.

[37] M. Spira, Fortsch. Phys. **46**, 203 (1998), arXiv:hep-ph/9705337.

[38] A. Belyaev, A. Blum, R. S. Chivukula, and E. H. Simmons, Phys.Rev. **D72**, 055022 (2005), arXiv:hep-ph/0506086.

[39] A. Azatov, R. Contino, and J. Galloway, (2012), arXiv:1202.3415.

[40] S. Chatrchyan *et al.*, Physics Letters B **710**, 26 (2012).

[41] The ATLAS Collaboration, CERN Report No. ATLAS-CONF-2012-019, 2012 (unpublished).

[42] The CMS Collaboration, CERN Report No. CMS-PAS-HIG-12-015, 2012 (unpublished).

[43] The CMS Collaboration, CERN Report No. CMS-PAS-HIG-12-016, 2012 (unpublished).

[44] G. Belanger, N. D. Christensen, A. Pukhov, and A. Semenov, (2010), arXiv:1008.0181.

Appendix A: Feynman rules

Below is a table of the Feynman rules for the propagators and vertices needed to evaluate the diagrams contributing to the $gg \to h$ and $h \to \gamma\gamma$ amplitudes. The vertex rules are given in terms of a general coefficient; underneath this, the value of the coefficient is written for the SM case and for the nth KK level. We use a $(+---)$ signature and the following momentum conventions: fermion momentum flows in the same direction as fermion number and external momentum flows inwards. This convention is shown graphically in Fig. 1

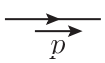

$$= \frac{\mathrm{i}(\not{p} + m)}{p^2 - m^2 + \mathrm{i}\epsilon}$$

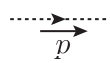

$$= \frac{\mathrm{i}}{p^2 - m^2 + \mathrm{i}\epsilon}$$

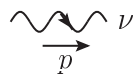

$$= \frac{-\mathrm{i}g_{\mu\nu}}{p^2 - m^2 + \mathrm{i}\epsilon} \text{ (Feynman gauge)}$$

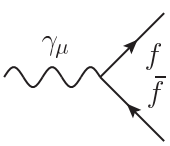

$$\mathrm{i}G_{ff}\gamma_\mu$$

$$G_{ff}^{\mathrm{SM}} = -eQ_f$$

$$G_{ff}^{(n)} = -eQ_f$$

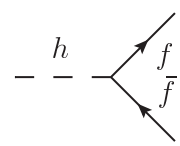

$$\mathrm{i}\lambda_{ff}$$

$$\lambda_{ff}^{\mathrm{SM}} = -\frac{gm_f}{2m_W}$$

$$\lambda_{ff}^{(n)} = -\frac{gm_f}{2m_W}\sin 2a_f^{(n)}$$

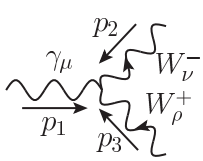

$$\mathrm{i}G_{WW}(p_{3\mu}g_{\nu\rho} - p_{3\nu}g_{\mu\rho} - p_{1\rho}g_{\mu\nu} + p_{1\nu}g_{\mu\rho} + p_{2\rho}g_{\mu\nu} - p_{2\mu}g_{\nu\rho})$$

$$G_{WW}^{\mathrm{SM}} = -e$$

$$G_{WW}^{(n)} = -e$$

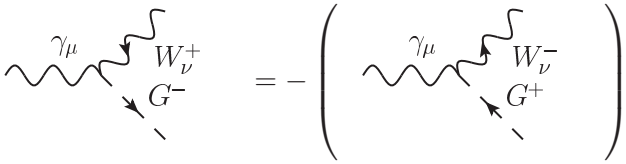

$$G_{WG} g_{\mu\nu}$$

$$G_{WG}^{\mathrm{SM}} = e m_W$$

$$G_{WG}^{(n)} = e m_{W,n}$$

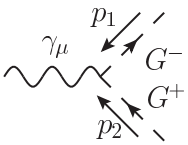

$$\mathrm{i}G_{GG}(p_2 - p_1)_\mu$$

$$G_{GG}^{\mathrm{SM}} = e$$

$$G_{GG}^{(n)} = e$$

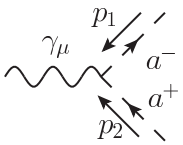

$$\mathrm{i}G_{aa}(p_2 - p_1)_\mu$$

$$G_{aa}^{\mathrm{SM}} = 0$$

$$G_{aa}^{(n)} = e$$

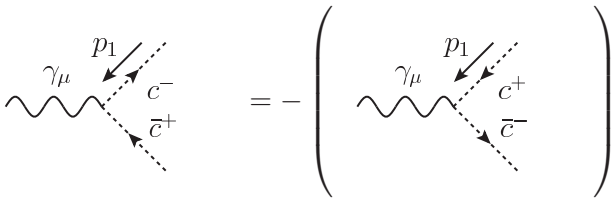

$$\mathrm{i}G_{\bar{c}c} p_{1\mu}$$

$$G_{\bar{c}c}^{\mathrm{SM}} = -e$$

$$G_{\bar{c}c}^{(n)} = -e$$

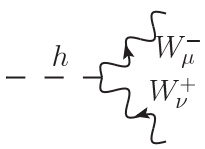

$$\mathrm{i}\lambda_{WW} g_{\mu\nu}$$

$$\lambda_{WW}^{\mathrm{SM}} = g m_W$$

$$\lambda_{WW}^{(n)} = g m_W$$

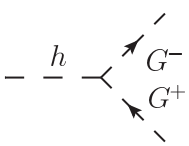

$$\mathrm{i}\lambda_{GG}$$

$$\lambda_{GG}^{\mathrm{SM}} = -g m_h^2/(2m_W)$$

$$\lambda_{GG}^{(n)} = -\frac{g m_h^2}{2m_W}\left(\frac{m_W}{m_{W,n}}\right)^2$$

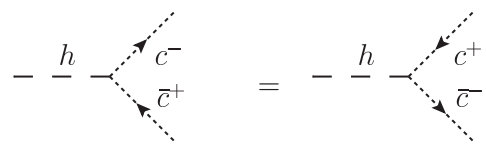

$$\mathrm{i}\lambda_{\bar{c}c}$$

$$\lambda_{\bar{c}c}^{\mathrm{SM}} = -gm_W/2$$

$$\lambda_{\bar{c}c}^{(n)} = -gm_W/2$$

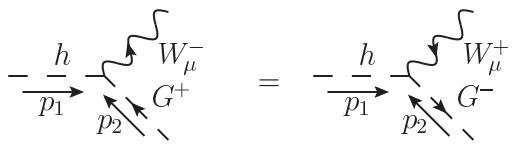

$$-\lambda_{WG}(p_2 - p_1)_\mu$$

$$\lambda_{WG}^{\mathrm{SM}} = -g/2$$

$$\lambda_{WG}^{(n)} = -(g/2)(m_W/m_{W,n})$$

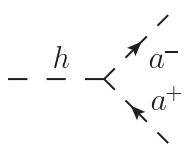

$$\mathrm{i}\lambda_{aa}$$

$$\lambda_{aa}^{\mathrm{SM}} = 0$$

$$\lambda_{aa}^{(n)} = -\frac{g}{2m_W}\left[2\left(\frac{m_{a,n}}{m_{W,n}}\right)^2 m_W^2 + m_h^2\left(1 - \frac{m_W^2}{m_{W,n}^2}\right)\right]$$

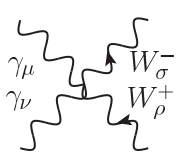

$$\mathrm{i}H_{WW}(2g_{\mu\nu}g_{\rho\sigma} - g_{\mu\sigma}g_{\nu\rho} - g_{\mu\rho}g_{\nu\sigma})$$

$$H_{WW}^{\mathrm{SM}} = -e^2$$

$$H_{WW}^{(n)} = -e^2$$

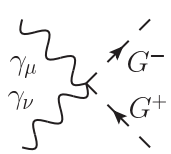

$$\mathrm{i}H_{GG}g_{\mu\nu}$$

$$H_{GG}^{\mathrm{SM}} = 2e^2$$

$$H_{GG}^{(n)} = 2e^2$$

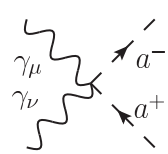

$$\mathrm{i}H_{aa}g_{\mu\nu}$$

$$H_{aa}^{\mathrm{SM}} = 0$$

$$H_{aa}^{(n)} = 2e^2$$

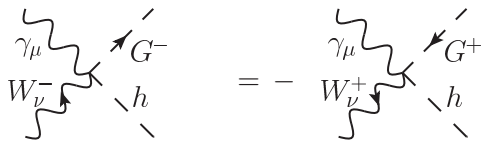

$$I_{WG} g_{\mu\nu}$$

$$I_{WG}^{\rm SM} = -\frac{eg}{2}$$

$$I_{WG}^{(n)} = -\frac{eg}{2}\frac{m_W}{m_{W,n}}$$

Appendix B: $gg \to h$ **amplitude**

Here we calculate the generic 1-loop amplitude for two gluons to produce a Higgs boson via a quark loop. We leave the couplings and quark masses general for now and will specialise to the SM and mUED case below.

$$\mathrm{i}(\mathcal{A}_{ggh,q})^{ab}_{\mu\nu} = 2 \times$$

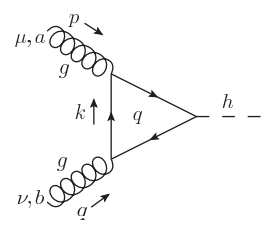

The factor of two is to count the diagram formed by swapping the external gluons. To form the amplitude above diagram should be contracted with the gluon polarisation vectors which carry Lorentz and group indices. The labeled arrows denote momentum flow; the other labels designate the particle names.

The KK and SM quarks couple to gluons identically as $\mathrm{i}g_s t_a$, where g_s is the strong coupling constant and t^a is an SU(3) generator. We call the Yukawa coupling $\mathrm{i}\lambda_q$.

Performing the loop momentum integral in $D = 4 - \epsilon$ dimensions to regulate the divergence (and introducing the renormalisation scale μ to compensate), the amplitude without polarisation vectors is

$$\begin{aligned}\mathrm{i}(\mathcal{A}_{ggh,q})^{ab}_{\mu\nu} &= -2(\mathrm{i}g_s)^2(\mathrm{i}\lambda_q)\mathrm{Tr}(t^a t^b)\mu^{4-D} \\ &\quad \times \int \frac{\mathrm{d}^D k}{(2\pi)^D}\mathrm{tr}\left\{\frac{\mathrm{i}(\not{k}+m)}{k^2-m^2+\mathrm{i}\epsilon}\gamma_\mu \frac{\mathrm{i}(\not{k}+\not{p}+m)}{(k+p)^2-m^2+\mathrm{i}\epsilon}\frac{\mathrm{i}(\not{k}-\not{q}+m)}{(k-q)^2-m^2+\mathrm{i}\epsilon}\gamma_\nu\right\}\end{aligned}$$

with the overall minus sign due to the fermion loop. The propagator conventions used here are given in appendix A with the mass set to a general quark mass m (we reserve the symbol m_q for the SM mass

of quark q). The trace Tr is over the SU(3) generators and tr is over the product of Dirac matrices.

The rest of the calculation (and all following calculations) assumes that the gluons and Higgs boson are physical, so $p^2 = q^2 = 0$, $p^\mu \epsilon_\mu(p) = q^\nu \epsilon_\nu(q) = 0$ and $(p+q)^2 = m_h^2$. The approximation that the Higgs is real is justified if the "narrow width approximation" is valid (see Sec. III for details).

The numerator of the Dirac trace (rejecting off-shell terms as discussed above) is

$$\mathrm{i}^3 \times 4m[g_{\mu\nu}(m^2 - k^2 - m_h^2/2) + 4k_\mu k_\nu + p_\nu q_\mu] = \mathrm{i}^3 \times 4m\{[(m^2 - m_H^2/2)g_{\mu\nu} + p_\nu q_\mu] - g_{\mu\nu}k^2 + 4k_\mu k_\nu\}.$$

In terms of PV functions the amplitude becomes

$$\mathrm{i}(\mathcal{A}_{ggh,q})^{ab}_{\mu\nu} = -2(\mathrm{i}g_s)^2(\mathrm{i}\lambda_q)\mathrm{Tr}(t^a t^b)\mathrm{i}^3\frac{\mathrm{i}\pi^2}{(2\pi)^4}4m\left\{[(m^2 - m_h^2/2)g_{\mu\nu} + p_\nu q_\mu]C_0 + g_{\mu\nu}C^\rho_\rho + 4C_{\mu\nu}\right\}.$$

Performing Passarino-Veltman reduction, and carefully taking the limit $D \to 4$, we find that

$$\mathrm{i}(\mathcal{A}_{ggh,q})^{ab}_{\mu\nu} = \frac{\mathrm{i}}{2\pi^2}\lambda_q g_s^2 \mathrm{Tr}(t^a t^b) m\left(\frac{g_{\mu\nu}m_h^2}{2} - p_\nu q_\mu\right)\left[\frac{2}{m_h^2} - \left(1 - \frac{4m^2}{m_h^2}\right)C_0\right].$$

For SU(3) generators, $\mathrm{Tr}(t^a t^b) = \frac{1}{2}\delta^{ab}$ so the quark q's total contribution to the amplitude is

$$\mathrm{i}(\mathcal{A}_{ggh,q})^{ab}_{\mu\nu} = \frac{\mathrm{i}\alpha_s}{\pi}\delta^{ab}\left(\frac{g_{\mu\nu}m_h^2}{2} - p_\nu q_\mu\right)\lambda_q m\left[\frac{2}{m_h^2} - \left(1 - \frac{4m^2}{m_h^2}\right)C_0(m, m_h)\right],$$

where $\alpha_s = g_s^2/4\pi$.

It is useful to factor out the Lorentz and colour dependence by defining the "reduced amplitude" $\tilde{\mathcal{A}}$ for a particular process in terms of the the full (*sans* polarisation vectors) amplitude $\mathcal{A}^{ab}_{\mu\nu}$:

$$\mathcal{A}^{ab}_{\mu\nu} = \tilde{\mathcal{A}} \times \delta^{ab}\left(\frac{g_{\mu\nu}m_h^2}{2} - p_\nu q_\mu\right),$$

so in this case

$$\tilde{\mathcal{A}}_{ggh,q} = \frac{\alpha_s}{\pi}\lambda_q m\left[\frac{2}{m_h^2} - \left(1 - \frac{4m^2}{m_h^2}\right)C_0(m, m_h)\right],$$

which can be written in terms of the function defined in (5) as

$$\tilde{\mathcal{A}}_{ggh,q} = \frac{\alpha_s}{4\pi}\lambda_q \frac{1}{m} f_F(m). \tag{B1}$$

1. The SM and mUED cases

a. *Standard Model*

Equation (B1) is in terms of the mass m and Yukawa coupling λ_q of a general quark q. For the SM quarks, let $m = m_q$ with $q \in \{u, d, s, c, b, t\}$. The SM Yukawa coupling in terms of the Higgs vacuum

expectation value (VEV) v is $\lambda_q^{\rm SM} = -m_q/v$, so

$$\tilde{\mathcal{A}}_{ggh}^{\rm SM} = -\frac{\alpha_s}{4\pi v} F_{ggh}^{\rm SM},$$

where

$$F_{ggh}^{\rm SM} = \sum_q f_{\rm F}(m_q), \tag{B2}$$

which is the expression shown in (4) and the following paragraph in Sec. III.

b. Including KK modes

At each KK level n, there are two types of quarks $q_1^{(n)}$ and $q_2^{(n)}$ for each SM quark q. At tree level, these quarks' masses would both be $\sqrt{m_q^2 + n^2/R^2}$, but if one-loop mass corrections are included then they split. However, Yukawa couplings to the Higgs are shifted equally under mass corrections so $\lambda_q^{(n)} = -m_q \sin(2a_q^{(n)})/v$ for both $q_1^{(n)}$ and $q_2^{(n)}$. Here $a_q^{(n)}$ is the mixing angle between quark flavour eigenstates $(q_L^{(n)}, q_R^{(n)})$ and mass eigenstates $(q_1^{(n)}, q_2^{(n)})$; this is explained further in [16].

The contribution to $\tilde{\mathcal{A}}_{ggh}$ from the KK level n quarks is then $\tilde{\mathcal{A}}_{ggh}^{(n)} = -\frac{\alpha_s}{4\pi v} F_{ggh}^{(n)}$, where

$$F_{ggh}^{(n)} = \sum_q \sin(2a_q^{(n)}) \left(\frac{m_q}{m_{q,1}^{(n)}} f_F(m_{q,1}^{(n)}, m_h) + \frac{m_q}{m_{q,2}^{(n)}} f_F(m_{q,2}^{(n)}, m_h) \right).$$

The full expression for F_{ggh} (and hence $\tilde{\mathcal{A}}_{ggh}$), as given in (7), is obtained by summing over the KK number n and adding the SM contribution (B2).

Appendix C: $h \to \gamma\gamma$ amplitude

The full $h \to \gamma\gamma$ amplitude receives contributions from fermions (quarks and leptons), W bosons and charged scalars $a^\pm$ (which appear at KK number 1 and above). We use the subscript f, W and a to distinguish these contributions.

1. Fermion contribution

For each fermion there are two contributing diagrams (equal to each other and related by the swapping external photons).

$\mathrm{i}(\mathcal{A}_f)_{\mu\nu} = 2 \times$

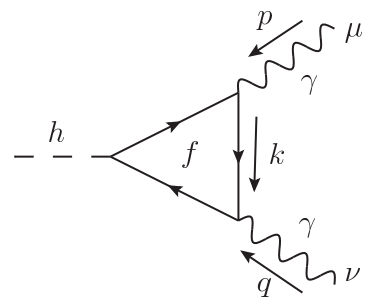

Leaving the couplings general and using the Feynman rules in Appendix A we find that

$$\begin{aligned}\mathrm{i}(\mathcal{A}_f)_{\mu\nu} &= -2(+\mathrm{i}G_{ff})^2(+\mathrm{i}\lambda_{ff})(+\mathrm{i})^3 \int_k \frac{1}{\mathcal{D}} \mathrm{tr}[(\not{k}+m)\gamma_\mu(\not{k}+\not{p}+m)(\not{k}-\not{q}+m)\gamma_\nu] \\ &= \frac{2\mathrm{i}G_{ff}^2\lambda_{ff}}{16\pi^2}\left[4\frac{m}{m_h^2}(4m^2-m_h^2)C_0 + \frac{8m}{m_h^2}\right]\left(\frac{m_h^2 g_{\mu\nu}}{2} - p_\nu q_\mu\right).\end{aligned}$$

where we have used the shorthand

$$\int_k \equiv \int \frac{\mathrm{d}^D k}{(2\pi)^D}\mu^{4-D}$$

for the dimensionally-regularised momentum integral and where we have written the denominator, common to all triangle diagrams considered in this paper, as

$$\mathcal{D} = [k^2 - m^2 + \mathrm{i}\epsilon][(k+p)^2 - m^2 + \mathrm{i}\epsilon][(k-q)^2 - m^2 + \mathrm{i}\epsilon].$$

Factoring out the Lorentz part yields as in the ggh case leaves

$$\tilde{\mathcal{A}}_f = \frac{G_{ff}^2\lambda_{ff}}{8\pi^2}\frac{1}{m}f_F(m),$$

with $f_F(m)$ defined as in (5).

Specialising to the SM using the rules in Appendix A gives

$$\tilde{\mathcal{A}}_f^{\mathrm{SM}} = -\frac{Q_f^2 e^2}{8\pi^2 v}f_F(m_f),$$

where $v = 2m_W/g$ is the Higgs VEV and $Q_f e$ is the charge of the fermion.

The contribution from an nth level KK fermion is

$$\tilde{\mathcal{A}}_f^{(n)} = -\frac{Q_f^2 e^2}{8\pi^2 v}\sin 2a_f^{(n)} f_F(m_f^{(n)}),$$

where $a_f^{(n)}$ is the mixing angle for converting from the flavour to the mass eigenbasis of the KK fermion.

2. Gauge boson contribution

There is an additional (in fact dominant) contribution to the $h \to \gamma\gamma$ amplitude from SM and KK W bosons and their associated Goldstone bosons and Faddeev-Popov ghosts. We chose to perform the calculation in the 't Hooft-Feynman gauge (the R_ξ gauge with $\xi = 1$). The relevant diagrams, including Goldstone (dashed) and ghost (dotted) internal lines, are as follows.

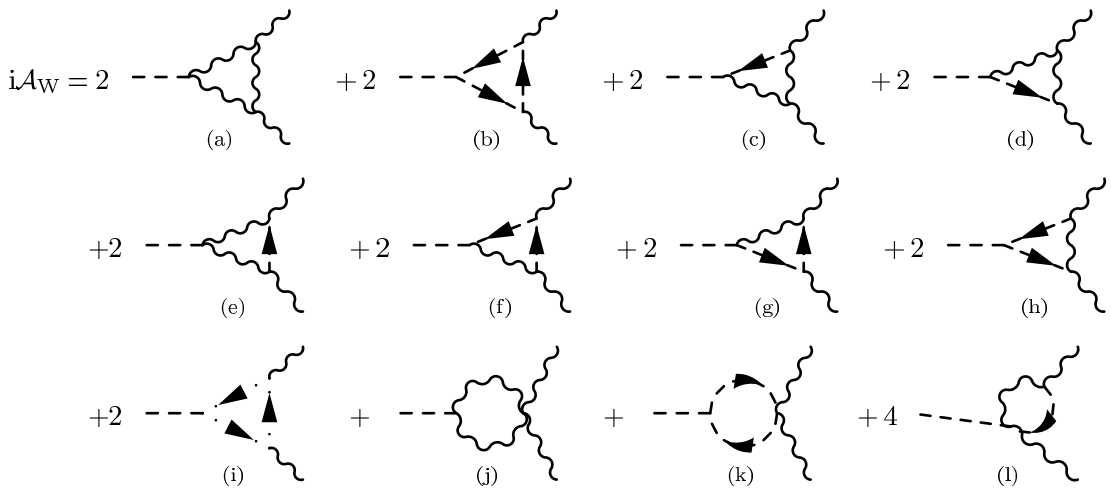

In the following we calculate the general expression for each diagram in turn and the corresponding SM and nth KK level expressions using the values for the couplings in Sec. A.

There are two W diagrams (related by crossing the external photons):

$$
\begin{aligned}
\mathrm{i}(\mathcal{A}_a)_{\mu\nu} &= 2\times(\mathrm{i}G_{WW})^2(\mathrm{i}\lambda_{WW})(-\mathrm{i})^3\int_k \frac{1}{\mathcal{D}} g^{\rho\sigma}[-(k+p)_\mu g_{\sigma\lambda}+(k+p)_\sigma g_{\mu\lambda}-p_\lambda g_{\mu\sigma}+p_\sigma g_{\mu\lambda} \\
&\quad + k_\lambda g_{\mu\sigma}-k_\mu g_{\sigma\lambda}]g^{\lambda\kappa}g_{\kappa\alpha}g^{\alpha\beta}[-k_\nu g_{\beta\rho}+k_\beta g_{\nu\rho}-q_\rho g_{\nu\beta}+q_\beta g_{\nu\rho}+(k-q)_\rho g_{\nu\beta}-(k-q)_\nu g_{\beta\rho}] \\
&= 2G_{WW}^2\lambda_{WW}\frac{\mathrm{i}\pi^2}{(2\pi)^4}[2g_{\mu\nu}g^{\rho\sigma}C_{\rho\sigma}+g_{\mu\nu}(p-q)^\rho C_\rho-\frac{5g_{\mu\nu}m_h^2}{2}C_0+10C_{\mu\nu}+p_\nu C_\mu-q_\mu C_\nu \\
&\qquad\qquad + 4p_\nu q_\mu C_0] \\
&= \frac{\mathrm{i}G_{WW}^2\lambda_{WW}}{8\pi^2}[2Dg_{\mu\nu}C_{00}-2m_h^2 g_{\mu\nu}C_{12}-g_{\mu\nu}m_h^2 C_1-\frac{5g_{\mu\nu}m_h^2}{2}C_0+10g_{\mu\nu}C_{00}-10p_\nu q_\mu C_{12} \\
&\qquad\qquad - 2p_\nu q_\mu C_1+4p_\nu q_\mu C_0] \\
&= \frac{\mathrm{i}G_{WW}^2\lambda_{WW}}{8\pi^2}\Bigg[\left(Dm^2 g_{\mu\nu}+3m^2 g_{\mu\nu}-\frac{5}{2}m_h^2 g_{\mu\nu}-\frac{10m^2 p_\nu q_\mu}{m_h^2}+4p_\nu q_\mu\right)C_0 \\
&\quad + \left(\frac{1}{2}Dg_{\mu\nu}-\frac{2p_\nu q_\mu}{m_h^2}+\frac{3}{2}g_{\mu\nu}\right)B_0(m_h^2,m^2)+\left(g_{\mu\nu}+\frac{2p_\nu q_\mu}{m_h^2}\right)B_0(0,m^2)+\frac{Dg_{\mu\nu}}{2}+\frac{3g_{\mu\nu}}{2} \\
&\quad - \frac{5p_\nu q_\mu}{m_h^2}\Bigg] \\
&= \frac{\mathrm{i}G_{WW}^2\lambda_{WW}}{8\pi^2}\Bigg[\left(4m^2 g_{\mu\nu}+3m^2 g_{\mu\nu}-\frac{5}{2}m_h^2 g_{\mu\nu}-\frac{10m^2 p_\nu q_\mu}{m_h^2}+4p_\nu q_\mu\right)C_0 \\
&\quad + \left(2g_{\mu\nu}-\frac{2p_\nu q_\mu}{m_h^2}+\frac{3}{2}g_{\mu\nu}\right)B_0(m_h^2,m^2)+\left(g_{\mu\nu}+\frac{2p_\nu q_\mu}{m_h^2}\right)B_0(0,m^2)+\frac{5g_{\mu\nu}}{2} \\
&\quad - \frac{5p_\nu q_\mu}{m_h^2}\Bigg].
\end{aligned}
$$

Throughout the calculation we work in $D=4-\epsilon$ dimensions except for the last equality where we take the $\epsilon\to 0^+$ limit. Care must be taken in the case of the first B_0 function:

$$
\lim_{\epsilon\to 0^+}[DB_0(m_h^2,m^2)] = 4\lim_{\epsilon\to 0^+}[B_0(m_h^2,m^2)]-2;
$$

this is the origin of the extra $-g_{\mu\nu}$ term in the last line.

The two Goldstone loop diagrams evaluate to

$$
\begin{aligned}
\mathrm{i}(\mathcal{A}_b)_{\mu\nu} &= 2\times(\mathrm{i}G_{GG})^2(\mathrm{i}\lambda_{GG})(+\mathrm{i})^3\int_k \frac{1}{\mathcal{D}}[-(k+p)-k]_\mu[-k-(k-q)]_\nu \\
&= -2G_{GG}^2\lambda_{GG}\frac{\mathrm{i}\pi^2}{(2\pi)^4}4C_{\mu\nu} \\
&= -\frac{\mathrm{i}G_{GG}^2\lambda_{GG}}{2\pi^2}(C_{00}g_{\mu\nu}-p_\nu q_\mu C_{12}) \\
&= -\frac{\mathrm{i}G_{GG}^2\lambda_{GG}}{2\pi^2}\left[\left(\frac{m^2 g_{\mu\nu}}{2}-\frac{m^2 p_\nu q_\mu}{m_h^2}\right)C_0+\frac{g_{\mu\nu}}{4}B_0(m_h^2,m^2)+\left(\frac{g_{\mu\nu}}{4}-\frac{p_\nu q_\mu}{2m_h^2}\right)\right].
\end{aligned}
$$

There are 3×2 diagrams with two Ws and one Goldstone. The first four give[7]

$$
\begin{aligned}
\mathrm{i}(\mathcal{A}_c)_{\mu\nu} = \mathrm{i}(\mathcal{A}_d)_{\mu\nu} &= 2 \times (-G_{WG})(\lambda_{WG})(\mathrm{i}G_{WW})(-\mathrm{i})^2(+\mathrm{i}) \int_k \frac{1}{\mathcal{D}} g^{\rho\sigma} g_{\mu\sigma}[-(p+q)-(k+p)]_\lambda \\
&\quad \times g^{\lambda\kappa}[-k_\nu g_{\kappa\rho} + k_\kappa g_{\nu\rho} - q_\rho g_{\nu\kappa} + q_\kappa g_{\nu\rho} + (k-q)_\rho g_{\nu\kappa} - (k-q)_\nu g_{\kappa\rho}] \\
&= \frac{\mathrm{i}G_{WG}G_{WW}\lambda_{WG}}{8\pi^2} \\
&\quad \times [g_{\mu\nu}g^{\rho\sigma}C_{\rho\sigma} + 2g_{\mu\nu}(p+q)^\rho C_\rho + g_{\mu\nu}m_h^2 C_0 - C_{\mu\nu} + 2p_\nu C_\mu - 4q_\mu C_\nu - 4p_\nu q_\mu C_0] \\
&= \frac{\mathrm{i}G_{WG}G_{WW}\lambda_{WG}}{8\pi^2}[(D-1)g_{\mu\nu}C_{00} - (m_h^2 g_{\mu\nu} - p_\nu q_\mu)C_{12} + (m_h^2 g_{\mu\nu} - 4p_\nu q_\mu)C_1 \\
&\quad - (m_h^2 g_{\mu\nu} + 2p_\nu q_\mu)C_2 + (m_h^2 g_{\mu\nu} - 4p_\nu q_\mu)C_0] \\
&= \frac{\mathrm{i}G_{WG}G_{WW}\lambda_{WG}}{8\pi^2}\Bigg[\left(\frac{(D-1)g_{\mu\nu}}{4} - \frac{6p_\nu q_\mu}{m_h^2}\right)B_0(m_h^2, m^2) + \frac{6p_\nu q_\mu}{m_h^2}B_0(0, m^2) \\
&\qquad + \left(\frac{(D-3)}{2}m^2 g_{\mu\nu} + m_h^2 g_{\mu\nu} + \frac{m^2}{m_h^2}p_\nu q_\mu - 4p_\nu q_\mu\right)C_0 + \frac{(D-3)g_{\mu\nu}}{4} + \frac{p_\nu q_\mu}{2m_h^2}\Bigg] \\
&= \frac{\mathrm{i}G_{WG}G_{WW}\lambda_{WG}}{8\pi^2}\Bigg[\left(\frac{3}{4}g_{\mu\nu} - \frac{6p_\nu q_\mu}{m_h^2}\right)B_0(m_h^2, m^2) - \frac{g_{\mu\nu}}{2} + \frac{6p_\nu q_\mu}{m_h^2}B_0(0, m^2) \\
&\qquad \left(\frac{m^2}{2}g_{\mu\nu} + m_h^2 g_{\mu\nu} + \frac{m^2}{m_h^2}p_\nu q_\mu - 4p_\nu q_\mu\right)C_0 + \frac{g_{\mu\nu}}{4} + \frac{p_\nu q_\mu}{2m_h^2}\Bigg].
\end{aligned}
$$

The second two yield

$$
\begin{aligned}
\mathrm{i}(\mathcal{A}_e)_{\mu\nu} &= 2 \times (G_{WG})(-G_{WG})(\mathrm{i}\lambda_{WW})(\mathrm{i})(-\mathrm{i})^2 \int_k \frac{1}{\mathcal{D}} \left(g_{\mu\rho}g^{\rho\sigma}g_{\sigma\lambda}g^{\lambda\kappa}g_{\kappa\nu}\right) \\
&= \frac{\mathrm{i}\lambda_{WW}G_{Wf}^2 g^{\mu\nu}}{8\pi^2}C_0.
\end{aligned}
$$

[7] As in the case of $\tilde{\mathcal{A}}_a$, one must be careful when taking the $D \to 4$ limit in the last equality.

There are similarly 3×2 diagrams involving one W and two Goldstones. The first four evaluate to

$$\begin{aligned}
\mathrm{i}(\mathcal{A}_f)_{\mu\nu} = \mathrm{i}(\mathcal{A}_g)_{\mu\nu} &= 2 \times (\mathrm{i}G_{GG})(\lambda_{WG})(-G_{WG})(+\mathrm{i})^2(-\mathrm{i}) \\
&\quad \int_k \frac{1}{\mathcal{D}}[-(k+p)-k]_\mu[-(p+q)-(k+p)]_\rho g^{\rho\sigma} g_{\nu\sigma} \\
&= 2G_{GG}G_{WG}\lambda_{WG}\int_k \frac{1}{\mathcal{D}} 2k_\mu(2p+q+k)_\nu \\
&= \frac{\mathrm{i}G_{GG}G_{WG}\lambda_{WG}}{4\pi^2}(2p_\nu C_\mu + C_{\mu\nu}) \\
&= \frac{\mathrm{i}G_{GG}G_{WG}\lambda_{WG}}{4\pi^2}(-2p_\nu q_\mu C_1 + g_{\mu\nu}C_{00} - p_\nu q_\mu C_{12}) \\
&= \frac{\mathrm{i}G_{GG}G_{WG}\lambda_{WG}}{4\pi^2}\left[\left(\frac{m^2 g_{\mu\nu}}{2} - \frac{m^2 p_\nu q_\mu}{m_h^2}\right)C_0 + \left(\frac{g_{\mu\nu}}{4} - \frac{2p_\nu q_\mu}{m_h^2}\right)B_0(m_h^2, m^2)\right. \\
&\qquad \left. + \frac{2p_\nu q_\mu}{m_h^2}B_0(0, m^2) + \left(\frac{g_{\mu\nu}}{4} - \frac{p_\nu q_\mu}{2m_h^2}\right)\right]
\end{aligned}$$

while the other two give

$$\begin{aligned}
\mathrm{i}(\mathcal{A}_h)_{\mu\nu} &= 2 \times (-G_{WG})(+G_{WG})(+\mathrm{i}\lambda_{GG})(\mathrm{i})^2(-\mathrm{i})\int_k \frac{1}{\mathcal{D}} g^{\rho\sigma} g_{\mu\sigma} g_{\nu\rho} \\
&= \frac{\mathrm{i}\lambda_{GG}G_{WG}^2 g_{\mu\nu}}{8\pi^2}C_0.
\end{aligned}$$

The last triangle diagrams are the two involving Faddeev-Popov ghosts:

$$\begin{aligned}
\mathrm{i}(\mathcal{A}_i)_{\mu\nu} &= -2 \times (-\mathrm{i}G_{\bar{c}c})^2(+\mathrm{i}\lambda_{\bar{c}c})(+\mathrm{i})^3\int_k \frac{1}{\mathcal{D}}[-(k+p)]_\mu(-k)_\nu \\
&= 2G_{\bar{c}c}^2\lambda_{\bar{c}c}\frac{\mathrm{i}\pi^2}{(2\pi)^4}C_{\mu\nu} \\
&= \frac{\mathrm{i}G_{\bar{c}c}^2\lambda_{\bar{c}c}}{8\pi^2}\left(C_{00}g_{\mu\nu} - p_\nu q_\mu C_{12}\right) \\
&= \frac{\mathrm{i}G_{\bar{c}c}^2\lambda_{\bar{c}c}}{8\pi^2}\left[\left(\frac{m^2}{m_h^2}C_0 + \frac{1}{2m_h^2}\right)\left(\frac{m_h^2 g_{\mu\nu}}{2} - p_\nu q_\mu\right) + \frac{g_{\mu\nu}}{4}B_0(m_h^2, m^2)\right].
\end{aligned}$$

There are six remaining (non-triangle) diagrams involving four-point vertices. The W diagram evaluates to

$$\begin{aligned}
\mathrm{i}(\mathcal{A}_j)_{\mu\nu} &= (\mathrm{i}H_{WW})(\mathrm{i}\lambda_{WW})(-\mathrm{i})^2\int_k \frac{g^{\rho\sigma}}{k^2 - m^2 + \mathrm{i}\epsilon}g_{\sigma\lambda}\frac{g^{\lambda\kappa}}{(k-p-q)^2 - m^2 + \mathrm{i}\epsilon}(2g_{\mu\nu}g_{\kappa\rho} - g_{\mu\rho}g_{\nu\kappa} - g_{\mu\kappa}g_{\nu\rho}) \\
&= H_{WW}\lambda_{WW}2g_{\mu\nu}(D-1)\frac{\mathrm{i}\pi^2}{(2\pi)^4}B_0(m_h^2, m^2) \\
&= \frac{\mathrm{i}H_{WW}\lambda_{WW}(D-1)g_{\mu\nu}}{8\pi^2}B_0(m_h^2, m^2) \\
&= \frac{\mathrm{i}H_{WW}\lambda_{WW}g_{\mu\nu}}{8\pi^2}[3B_0(m_h^2, m^2) - 2],
\end{aligned}$$

and the Goldstone diagram evaluates to

$$\begin{aligned}\mathrm{i}(\mathcal{A}_k)_{\mu\nu} &= (\mathrm{i}H_{GG})(\mathrm{i}\lambda_{GG})(\mathrm{i})^2 g_{\mu\nu}\int_k \frac{1}{k^2-m^2+\mathrm{i}\epsilon}\frac{1}{(k-p-q)^2-m^2+\mathrm{i}\epsilon}\\ &= \frac{\mathrm{i}H_{GG}\lambda_{GG}g_{\mu\nu}}{16\pi^2}B_0(m_h^2,m^2).\end{aligned}$$

The last four diagrams are related to diagram (l) (shown above) by swapping external momenta and changing the direction of internal particle number flow:

$$\begin{aligned}\mathrm{i}(\mathcal{A}_l)_{\mu\nu} &= 4\times(-G_{WG})(+I_{WG})(-\mathrm{i})(+\mathrm{i})\int_k \frac{g^{\rho\sigma}g_{\mu\sigma}g_{\nu\rho}}{(k^2-m^2+\mathrm{i}\epsilon)[(k+p)^2-m^2+\mathrm{i}\epsilon]}\\ &= -\frac{\mathrm{i}G_{WG}I_{WG}g_{\mu\nu}}{4\pi^2}B_0(0,m^2).\end{aligned}$$

3. Summing the diagrams

We now need to sum the diagrams to find the SM and nth KK level contributions. We have checked the following expressions in `Mathematica`.

Putting in the SM values for masses and couplings gives the following. The Goldstone and ghost have the same mass as the W boson. (The same applies for the higher KK modes.)

$$\begin{aligned}\mathrm{i}(\mathcal{A}_W^{\mathrm{SM}})_{\mu\nu} &= \frac{3ie^2gm_h^2m_Wg_{\mu\nu}C_0}{8\pi^2}+\frac{3ie^2gm_W^3g_{\mu\nu}C_0}{4\pi^2}+\frac{3ie^2gm_Wp^\nu q^\mu C_0}{4\pi^2}-\frac{3ie^2gm_W^3p_\nu q_\mu C_0}{2\pi^2m_h^2}\\ &\quad+\frac{ie^2gm_h^2g_{\mu\nu}}{16\pi^2m_W}+\frac{3ie^2gm_Wg_{\mu\nu}}{8\pi^2}-\frac{3ie^2gm_Wp_\nu q_\mu}{4\pi^2m_h^2}-\frac{ie^2gp_\nu q_\mu}{8\pi^2m_W}.\end{aligned}$$

Factoring out the Lorentz part and writing things in terms of the dimensionless function f_V, defined in (13), gives

$$\tilde{\mathcal{A}}_W = -\frac{e^2g}{16\pi^2m_W}f_V(m_W).$$

The sum of the diagrams at the nth KK level is

$$\mathrm{i}(\mathcal{A}_W^{(n)})_{\mu\nu} = \frac{\mathrm{i}e^2gm_W}{8\pi^2m_h^2m_{W,n}^2}\left[m_h^2+6m_{W,n}^2+\left(12m_{W,n}^4-6m_h^2m_{W,n}^2\right)C_0\right]\left(\frac{m_h^2g_{\mu\nu}}{2}-p_\nu q_\mu\right),$$

so

$$\tilde{\mathcal{A}}_W^{(n)} = -\frac{e^2g}{16\pi^2m_W}\left(\frac{m_W}{m_{W,n}}\right)^2 f_V(m_{W,n}).$$

4. Scalar contribution

For KK number $n\geq 1$ there exist charged scalar particles $a_n^\pm$ not seen at the SM level. At tree level these have the same masses as their $W_n^\pm$ counterparts but loop corrections split this degeneracy.

There are three allowed diagrams at each KK level contributing to the $h \to \gamma\gamma$ amplitude that involve a charged scalar (two of them are numerically equal and are related by swapping the photon momenta):

$\mathrm{i}(\mathcal{A}^{(n)}_{a^\pm})_{\mu\nu} = 2 \times$

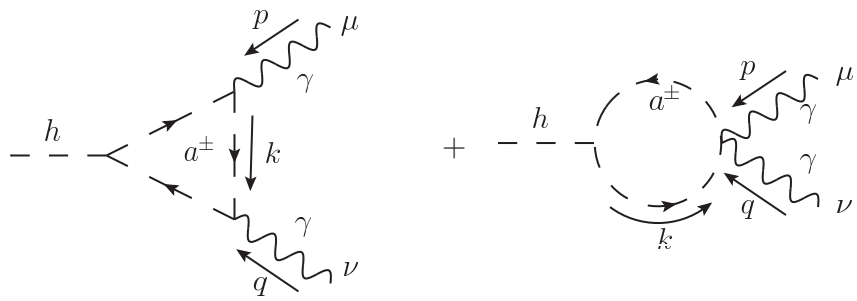

These diagrams are exactly the same as the similar Goldstone diagrams $\mathcal{A}_b$ and $\mathcal{A}_k$ evaluated in the previous section, but with a different particle mass and different couplings. Using the couplings from Sec. A, we get that

$$\begin{aligned}\mathrm{i}(\mathcal{A}^{(n)}_{a^\pm})_{\mu\nu} &= -\frac{2\mathrm{i}e^2\lambda_{aa}}{4\pi^2}\left[\left(\frac{m^2_{a,n}g_{\mu\nu}}{2} - \frac{m^2_{a,n}p_\nu q_\mu}{m_h^2}\right)C_0 + \frac{g_{\mu\nu}}{4} - \frac{p_\nu q_\mu}{2m_h^2}\right] \\ &= \frac{\mathrm{i}e^2 g}{4\pi^2 m_h^2 m_W}\left[2\frac{m^2_{a,n}}{m^2_{W,n}}m_W^2 + m_h^2\left(1 - \frac{m_W^2}{m^2_{W,n}}\right)\right]\left(\frac{1}{2} + m^2_{a,n}C_0\right)\left(\frac{m_h^2 g_{\mu\nu}}{2} - p_\nu q_\mu\right),\end{aligned}$$

so

$$\tilde{\mathcal{A}}^{(n)}_{a^\pm} = -\frac{e^2 g}{16\pi^2 m_W} f_S(m_{a,n}, m_{W,n}),$$

where $f_S(m_{a,n}, m_{W,n})$ is defined in (18).

Appendix D: P-V functions and conventions

1. Three-point PV function

The three-point scalar Passarino-Veltman function is frequently encountered when evaluating triangle diagrams. It is defined by

$$\frac{\mathrm{i}\pi^2}{(2\pi)^4}C_0(p^2, (p+q)^2, q^2, m_0^2, m_1^2, m_2^2) \equiv \mu^{4-D}\int \frac{\mathrm{d}^D k}{(2\pi)^D}\{(k^2 - m_0^2)[(k+p)^2 - m_1^2][(k-q)^2 - m_2^2]\}^{-1}.$$

We encounter this integral exclusively in the special case that the internal masses are equal:

$$\frac{\mathrm{i}\pi^2}{(2\pi)^4}C_0 \equiv \mu^{4-D}\int \frac{\mathrm{d}^D k}{(2\pi)^D}\frac{1}{\mathcal{D}},$$

where $\mathcal{D}$ is the denominator from the general expression with $m_0 = m_1 = m_2 \equiv m$:

$$\mathcal{D} = (k^2 - m_0^2)[(k+p)^2 - m^2][(k-q)^2 - m^2].$$

This integral can be evaluated [35] to give

$$C_0(m) = \begin{cases} -\frac{2}{m_h^2}\left[\arcsin\left(\frac{m_h}{2m}\right)\right]^2 & m^2 \geq m_h^2/4 \\ \frac{1}{2m_h^2}\left[\ln\left(\frac{1+\sqrt{1-4m^2/m_h^2}}{1-\sqrt{1-4m^2/m_h^2}}\right) - i\pi\right]^2 & m^2 < m_h^2/4. \end{cases} \tag{D1}$$

It is convenient to define a dimensionless version of this expression:

$$c_0(m) = -\frac{m_H^2}{2} C_0(m),$$

(where the normalisation matches the `fiRe` and `fiIm` functions defined in the `SLHAplus` library for `CalcHEP/MicrOMEGAS` [44]).

2. Two-point PV function

We also frequently come across the scalar two-point PV function:

$$\frac{\mathrm{i}\pi^2}{(2\pi)^4} B_0(p^2, m^2) \equiv \mu^{4-D} \int \frac{\mathrm{d}^D k}{(2\pi)^D} \{(k^2 - m^2)[(k+p)^2 - m^2]\}^{-1}.$$

We encounter the following two spacial cases

$$B_0(m_h^2, m^2) = \frac{1}{\bar{\epsilon}} - \ln\frac{m^2}{\mu^2} + 2 - \sqrt{1 - 4m^2/m_h^2}\sqrt{2m_h^2 C_0(m)} \tag{D2}$$

and

$$B_0(0, m^2) = \frac{1}{\bar{\epsilon}} - \ln\frac{m^2}{\mu^2}, \tag{D3}$$

with $D = 4 - \epsilon$ and

$$\frac{1}{\bar{\epsilon}} = \frac{2}{\epsilon} - \gamma_E - \ln\pi, \tag{D4}$$

$\gamma_E \approx 0.57721$ being the Euler-Mascheroni constant.

3. PV Reduction

More generally, we come across three-point momentum integrals with more complex Lorentz structure that can be written generically as

$$\frac{\mathrm{i}\pi^2}{(2\pi)^4} C^{\rho\sigma\ldots\kappa} \equiv \mu^{4-D} \int \frac{\mathrm{d}^D k}{(2\pi)^D} \frac{k^\rho k^\sigma \cdots k^\kappa}{\mathcal{D}}.$$

These can be simplified through *Passarino-Veltman reduction* to expressions involving the scalar three-point and two-point PV functions defined in (D1), (D2) and (D3); for on-shell external momenta (p^μ and q^ν) we get

$$\begin{aligned} C^{\mu\nu} &= g^{\mu\nu} C_{00} - p^\nu q^\mu C_{12} \\ g_{\rho\sigma} C^{\rho\sigma} &= D C_{00} - m_h^2 C_{12} \\ C^\mu &= -q^\mu C_2 \\ C^\nu &= p^\nu C_1. \end{aligned} \tag{D5}$$

The coefficient functions expand further to

$$\begin{aligned} C_{00} &= \frac{1}{2} m^2 C_0 + \frac{1}{4} B_0(m_h^2, m^2) + \frac{1}{4} \\ C_{12} &= \frac{m^2}{m_h^2} C_0 + \frac{1}{2 m_h^2} \\ C_1 = C_2 &= \frac{B_0\left(m_h^2, m^2\right)}{m_h^2} - \frac{B_0\left(0, m^2\right)}{m_h^2}. \end{aligned} \tag{D6}$$

We used the `PaVeReduce` function in the `FeynCalc` package for `Mathematica` to check this.

Ultimately one must take the $D \to 4$ limit. Particular care must be taken in the case of C_{00}:

$$\lim_{D \to 4} D C_{00} = 4 C_{00} + \lim_{\epsilon \to 0} \frac{\epsilon}{4\bar{\epsilon}} = 4 C_{00} + \frac{1}{2}.$$